UNCLASSIFIED

AD 282 439

Reproduced
by the

ARMED SERVICES TECHNICAL INFORMATION AGENCY
ARLINGTON HALL STATION
ARLINGTON 12, VIRGINIA

UNCLASSIFIED

282 439

DEVELOPMENT OF NONDESTRUCTIVE TESTING TECHNIQUES FOR LARGE SOLID-PROPELLANT ROCKET MOTORS

Engineering Division

United Technology Corporation

U
A
SUBSIDIARY OF UNITED AIRCRAFT CORPORATION

**FIRST TECHNICAL NOTE
1 MARCH THROUGH 30 JUNE 1962
UNDER CONTRACT No. AF 04(611)8018**

DEVELOPMENT OF NONDESTRUCTIVE TESTING TECHNIQUES

FOR

LARGE SOLID–PROPELLANT ROCKET MOTORS

Engineering Division
UNITED TECHNOLOGY CORPORATION
Sunnyvale, California

FIRST TECHNICAL NOTE
1 August 1962

Headquarters, Air Force Flight Test Center
Edwards Air Force Base, California

Prepared by:

    R. Citerley
    S. A. Murch
    D. Baker

Reviewed by: *Charles Harris*
Charles Harris
Project Engineer

Approved by: *A. C. Keathley*
A. C. Keathley
Manager
Solid Rocket Branch

ABSTRACT

This report summarizes the results of various analytical studies made under Contract AF 04(611)8018.

RELATIONSHIP OF EXCESS BURNING AREA AND CHAMBER PRESSURE. The relationship of chamber pressure to an arbitrary increase in burning area has been derived for propellants of various burning rate exponents by employing the basic relations of solid rocket motor combustion.

STRESS ANALYSIS OF THE PROPELLANT GRAIN. A method of analysis has been developed to determine the elastic stresses in a propellant grain subject to a constant body force and uniform temperature change. By two dimensional analog of a grain, a "stress concentration" factor for the end effects has been determined to be approximately 2-1/4 times the plane strain solution. Numerical results are presented for the 120-inch diameter motor.

STRESS CONCENTRATION DUE TO A VOID IN THE PROPELLANT GRAIN. The effect a void in the propellant grain has upon grain stresses has been developed.

PRESSURE DISTRIBUTION IN A PROPELLANT GRAIN CRACK. An investigation has been made of the pressure distribution due to burning within a crack in the propellant grain. For crack depth/width ratios exceeding 300, sonic flow at the crack exit is predicted.

MOTOR CASE HEATING. The problem of motor case heating due to premature web burnout has been investigated. Predicted values of motor case temperature versus time and insulation thickness are shown.

DETERMINATION OF SOLID PROPELLANT BURNING AREA FROM PRESSURE—TIME TRACE. A technique has been developed to evaluate the results of motor firings and calculate the actual burning area as a function of time.

TABLE OF CONTENTS

LIST OF ILLUSTRATIONS

LIST OF TABLES

LIST OF SYMBOLS

A = area

A_s = propellant burning surface area

a = inner radius, in.

b = constant in propellant burning rate law or outer radius, in.

C = specific heat

C_p = specific heat at constant pressure

C_v = specific heat at constant volume

D = differential operator

E = Young's Modulus of Elasticity, psi

g = gravitational constant at sea level

h = film coefficient

h_p = stagnation enthalpy of propellant gases

K = thermal conductivity

L = length, in., or thickness of insulation plus metal

M = Mach number

n = pressure exponent in burning rate law

P = pressure

P_c = chamber pressure

R = gas constant divided by molecular weight

r = radius, in., or propellant burning rate

T = temperature, $^\circ$F

T_A = initial temperature

T_c = flame temperature

T_m = metal slab temperature

T_w = wall temperature

t = time

U = complementary strain energy, in.–lb

U^* = modified complementary strain energy, in.–lb

u = deflection in x direction, in.

V = volume, cu in., or velocity of the gases parallel to x–axis

v = deflection in y direction, in.

$\dot{w}$ = flow rate

$\dot{w}_p$ = flow rate of propellant gases, entering control volume or leaving burning surface area

w = web thickness, in.

X_o = insulation thickness

X_{om} = metal slab thickness

x = distance

LIST OF SYMBOLS (Continued)

Greek Letters

α = coefficient of linear expansion, in./in./$^{\circ}$F

Γ = surface contour

γ = ratio of specific heats

ϵ = strain, in./in.

λ = characteristic roots

ν = Poisson's ratio

ξ = Lagrangian multiplier

ρ = density

ρ_b = propellant density

σ = normal stress, psi

τ = shear stress, psi

Subscripts

c = case

i = inlet properties from igniter

e = exit properties at nozzle throat

io = stagnation properties in the igniter

1 = properties at exit plane of nozzle

o = stagnation properties in motor combustion chamber

p = propellant

1.0 INTRODUCTION

In the course of satisfying the technical requirements of Contract AF 04(611)8018, a number of analytical studies were conducted. The purpose of this Technical Note is to present the results of the studies made to date. For the most part, these studies have been concerned with the defect-failure relationships in large solid propellant motors.

2.0 TECHNICAL DISCUSSION

2.1 RELATIONSHIP OF CHAMBER PRESSURE TO EXCESS BURNING AREA

The flow rate through a choked rocket motor nozzle is

$$\dot{w} = \frac{C P_c A_e}{\sqrt{T_c}} \qquad (1)$$

where

$$C = \sqrt{\frac{\gamma g}{R} \left(\frac{2}{\gamma+1}\right)^{\frac{\gamma+1}{\gamma-1}}} \quad .$$

The flow rate from the burning propellant surface area is

$$\dot{w} = \rho_b A_s \dot{r}$$

and assuming the experimental burning rate law of $\dot{r} = b P_c^n$, then

$$\dot{w} = \rho_b A_s b P_c^n \quad . \qquad (2)$$

For steady state conditions, the flow rates in Equations 1 and 2 must be equal. Thus,

$$P_c^{1-n} = \frac{b \rho_b A_s \sqrt{T_c}}{C A_e}$$

Letting the subscript "o" denote initial conditions, then

$$\frac{A_s}{A_{s_o}} = \left(\frac{P_c}{P_{c_o}}\right)^{1-n} \tag{3}$$

A graphical solution of Equation 3 for various burning rate exponents is given in Figure 1.

2.2 STRESS ANALYSIS OF THE PROPELLANT GRAIN

2.2.1 Introduction

An area of considerable importance in the design of solid propellant grains is that of three-dimensional linear elasticity. Many of the complex problems in this area are extremely involved and time consuming or they do not have known exact solutions. Therefore, simplifying assumptions or simpler approximate solutions are often necessary.

The effects of the ends on the stress distribution in a solid propellant grain due to thermal and gravitational loads is one of these complex problems. The application of classical two-dimensional elasticity in the analysis of a grain acted upon by these loads is well reported (References 1, 2, and 3). In order that these simplified solutions apply, an assumption is made that the area to be investigated is far from the ends of grain. Thus a condition of plane strain is assumed. But for the most part, these simplified analyses do not apply near the ends of the grain. Since it is well known to propellant manufacturers that bond failures near the end of a vertical standing propellant grain occur occasionally, a more detailed study is required for this very practical problem.
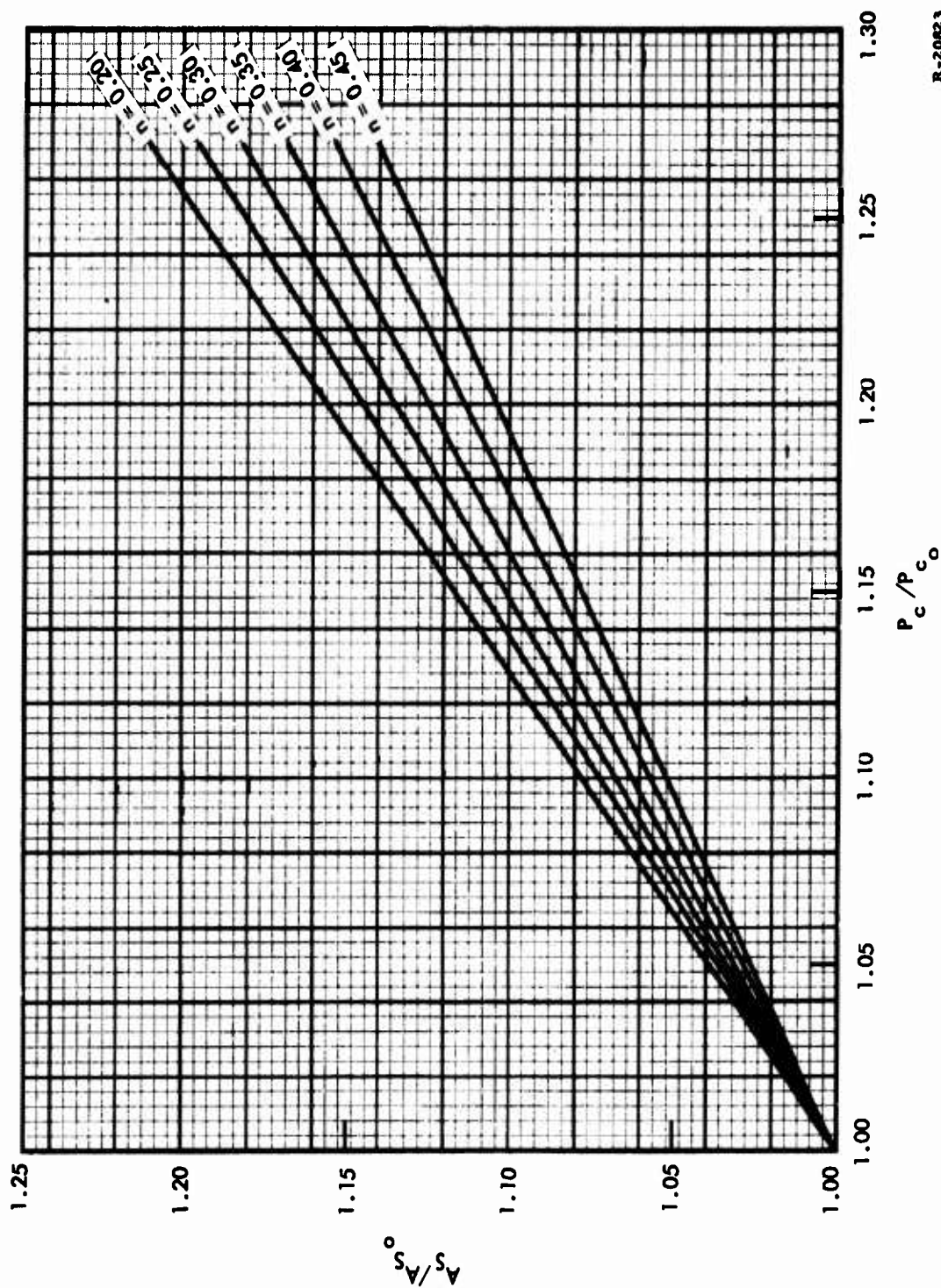
Figure 1. Surface Area — Chamber Pressure Relationship
for Various Burning Rate Exponents

R-20623

Some attempts have been made to obtain three dimensional elastic solutions to the end effects problem. Knauss (Reference 4) suggests that a variational method can be used if the form of the radial and axial deflections are assumed. By using the Fourier method suggested by Pickett (Reference 5), a form for the deflections is assumed. The behavior of the stress components along the boundary are then determined. Conte, Miller, Sensenig (Reference 6) and Messiner (Reference 7) attempted to solve the end effects problem through numerical procedures. Difference equations replace the differential equations of elasticity at discrete points in the grain. The stress components are predicted by using iterative techniques.

None of these suggested solutions provide complete correspondence to the original problem. If the form of the deflections are chosen as suggested by Knauss, complete satisfaction of equilibrium and/or the original boundary condition is not attained (i. e. deflection or stresses along certain boundaries are not maintained at specified values). Because of accuracy difficulties, the iterative techniques also do not completely satisfy the original boundary conditions. Therefore, a better understanding of end effects is required.

This presentation is separated into two sections. The first part deals primarily with the practical answers of bond stresses in a propellant grain. The second part presents the formal solution to the end effects problem.

2.2.2 Stresses in a Propellant Grain

Propellant, standing vertically being cured, can be ideally represented as an infinitely long hollow cylinder bonded at its outer radius to an elastically rigid case. The propellant is assumed to be elastic.

It is assumed that superposition principles remain valid. Therefore, the thermal loading resulting from cure and the gravity loading are assumed to be separable.

The stress free condition for the thermal loading is assumed to be at the cure temperature, T. As a result of the differences in co-efficients of linear expansion between the propellant and its casing, thermal stresses result when a uniform change in temperature, ΔT, is experienced.

The thermal elastic stress equations of <u>plane strain</u> for the propellant including the effect of polymerization are found to be (Sections 2.2.3 and 2.2.4):

$$\sigma_r = \Delta \frac{b^2}{a^2} \left[1 - \frac{a^2}{r^2} \right]$$

$$\sigma_\theta = \Delta \frac{b^2}{a^2} \left[1 + \frac{a^2}{r^2} \right] \qquad (4)$$

$$\sigma_z = \Delta \left[1 + \frac{b^2}{a^2} \right]$$

where

$$\Delta = E_p \left[(a_p - a_c) \Delta T + \frac{\Delta V}{3V} \right] \quad .$$

Near the ends of the cylinder, these stresses are altered drastically from the plane strain solution. To determine just how radical a change in stress distribution, the analogous two dimensional elasticity problem (Section 2.2.3) is examined.

At the ends of the cylinder an effective increase in maximum stress
or stress concentration factor is assumed to be the same as for the
two dimensional solution. The maximum stresses at the bond surface
have a magnitude

$$\sigma_r = 1.20\Delta \left(\frac{b^2}{a^2} - 1 \right)$$

$$\sigma_\theta = 1.70\,\Delta\,\frac{b^2}{a^2}$$

$$\sigma_z = 2.20\,\Delta \left(\frac{b^2}{a^2} + 1 \right)$$

$$\tau_{rz} = 1.40\,\Delta \left(\frac{b^2}{a^2} + 1 \right) .$$

(5)

Note that the end effects produce a shear stress not normally observed
by the plane strain solution.

The length of the cylinder can also be taken into account (Section 2.2.3),
thus giving rise to higher stress concentrations. For a length to web
thickness ratio of 3, the maximum stresses are:

$$\sigma_r = 1.20\Delta \left(\frac{b^2}{a^2} - 1 \right)$$

$$\sigma_\theta = 1.71\,\Delta\,\frac{b^2}{a^2}$$

$$\sigma_z = 2.21\,\Delta \left(\frac{b^2}{a^2} + 1 \right)$$

$$\tau_{rz} = 1.41\,\Delta \left(\frac{b^2}{a^2} + 1 \right)$$

(6)

A similar procedure for the gravitational loading results in the expressions:

$$\sigma_r = 0.870 \, \rho \, g \, b \left(1 - \frac{a^2}{b^2}\right)$$

$$\sigma_\theta = 0.430 \, \rho \, g \, b \left(1 - \frac{a^2}{b^2}\right)$$

$$\sigma_z = 0.870 \, \rho \, g \, b \left(1 - \frac{a^2}{b^2}\right) \tag{7}$$

$$\tau_{rz} = 0.77 \, \rho \, g \, b \left(1 - \frac{a^2}{b^2}\right) \quad .$$

The combined stresses due to gravity and thermal loading at the outer radius is simply the addition of Equations 6 and 7:

$$\sigma_r = \pm 1.2 \, \Delta \left(\frac{b^2}{a^2} - 1\right) \pm 0.870 \, \rho \, g \, b \left(1 - \frac{a^2}{b^2}\right)$$

$$\sigma_\theta = 1.71 \, \Delta \frac{b^2}{a^2} \pm 0.430 \, \rho \, g \, b \left(1 - \frac{a^2}{b^2}\right)$$

$$\sigma_z = 2.21 \, \Delta \left(\frac{b^2}{a^2} + 1\right) \pm 0.870 \, \rho \, g \, b \left(1 - \frac{a^2}{b^2}\right) \tag{8}$$

$$\tau_{rz} = 1.41 \, \Delta \left(\frac{b^2}{a^2} + 1\right) \pm 0.77 \, \rho \, g \, b \left(1 - \frac{a^2}{b^2}\right) \quad .$$

To obtain the principal stresses, the three normal stresses and the one shear stress are used. Since the shear stress, $\tau_{r\theta}$, is zero, one of the components in the $r\theta$ plane can be assumed to be a principal stress.

Assume $\sigma_3 < \sigma_2 < \sigma_1$
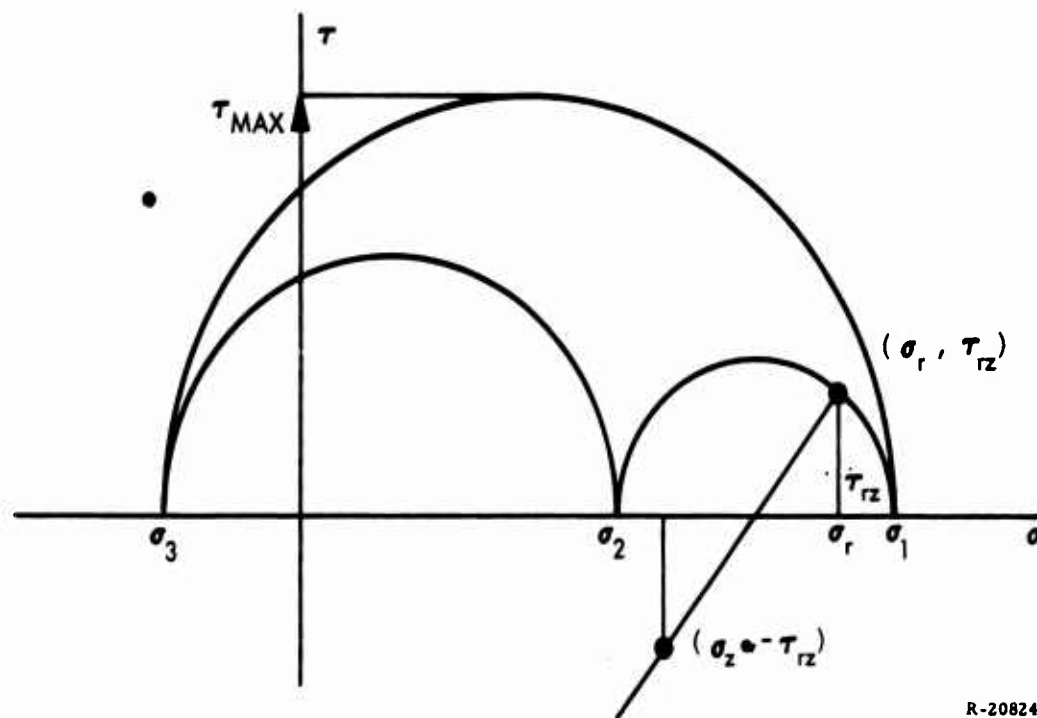
Figure 2. Mohr's Diagram

From Mohr's circle (Figure 2), the principal normal stresses, σ_1 and σ_2, can be determined

$$\sigma_{1,2} = \frac{\sigma_r + \sigma_z}{2} \pm \frac{1}{2} \sqrt{(\sigma_r - \sigma_z)^2 + 4\,T_{rz}^2} \ . \qquad (9)$$

The maximum shearing stress is therefore defined as

$$T_{max} = \frac{|\sigma_1| + |\sigma_3|}{2} \ . \qquad (10)$$

The use of the maximum shear criterion by no means implies the propellant material follows this failure phenomenon; it is to be used only as a guide. Further investigation as to the mode of failure is required before a failure criterion is chosen.

2.2.2.1 Application to 120-Inch Motor Grains

The assumed mechanical properties of PBAN propellant and physical dimensions for the 120-inch grain are as follows:

$$E_p = 300 \text{ psi}$$

$$a_p = 3.5 \times 10^{-5} \text{ in./in./°F}$$

$$\Delta T = 100 \text{°F}$$

$$\rho g = 0.063 \text{ lb/cu in.}^3$$

$$b = 60 \text{ in.}$$

$$a = 25 \text{ in.}$$

$$L = 60 \text{ in.}$$

$$\frac{\Delta V}{V} = 0.005$$

Substituting the above values into Equation 8, the stresses at the bond are obtained

$$\sigma_r = 10.44 \text{ psi}$$

$$\sigma_\theta = +11.14 \text{ psi}$$

$$\sigma_z = +17.64 \text{ psi}$$

$$\tau_{rz} = 11.92 \text{ psi}$$

Therefore, the principal stresses have values

$$\sigma_1 = 28.34 \text{ psi}$$

$$\sigma_2 = -1.0 \text{ psi}$$

and

$$\tau_{max} = \frac{|\sigma_1| + |\sigma_2|}{2} = 14.04 \text{ psi}$$

Note these maximum stresses occur at the top of a standing grain. The stresses at the bottom tend to cancel one another.

2.2.2.2 Effect of Boot at End of Grain

Effective use has been made of a relief at the end of a propellant grain in a form of a boot or cut formed wholly in the propellant liner. This boot allows a portion of the grain-case interface to be free during cure. Upon completion of cure, the void so created is filled with a compound such as an epoxy resin. This procedure is designed to keep the ends of the grain free of dangerous cracks.

If a body is free to move under a uniform temperature change, no stresses are induced in the body. Stresses, proportional to α_{est}, are induced when the body is completely restrained. The boot creates a stress condition somewhere between these two extremes. Since the modulus of most propellants is very low, the state of stress is more likely to be as in a free body rather than restrained. This also means that a case bonded cylinder of a length,

$$L' = L - 2B$$

where
L = length of original cylinder

B = length of boot or cut (one end) ,

can be assumed to stress free edges. From the effect of length analysis in Section 2.2.3, it is noted that (within limits) as the length of the cylinder decreases, the stress at the end increases. Thus, although the stresses at the extreme end of the cylinder have decreased, the stress at the base of the boot has increased. Figure 3 shows other stresses at the interface for L/W ratios of 2 and 3 for thermal loading; Figure 4, those for gravity loading.

There is one relieving factor when the boot is installed. After the grain has reached ambient conditions and after cure has taken
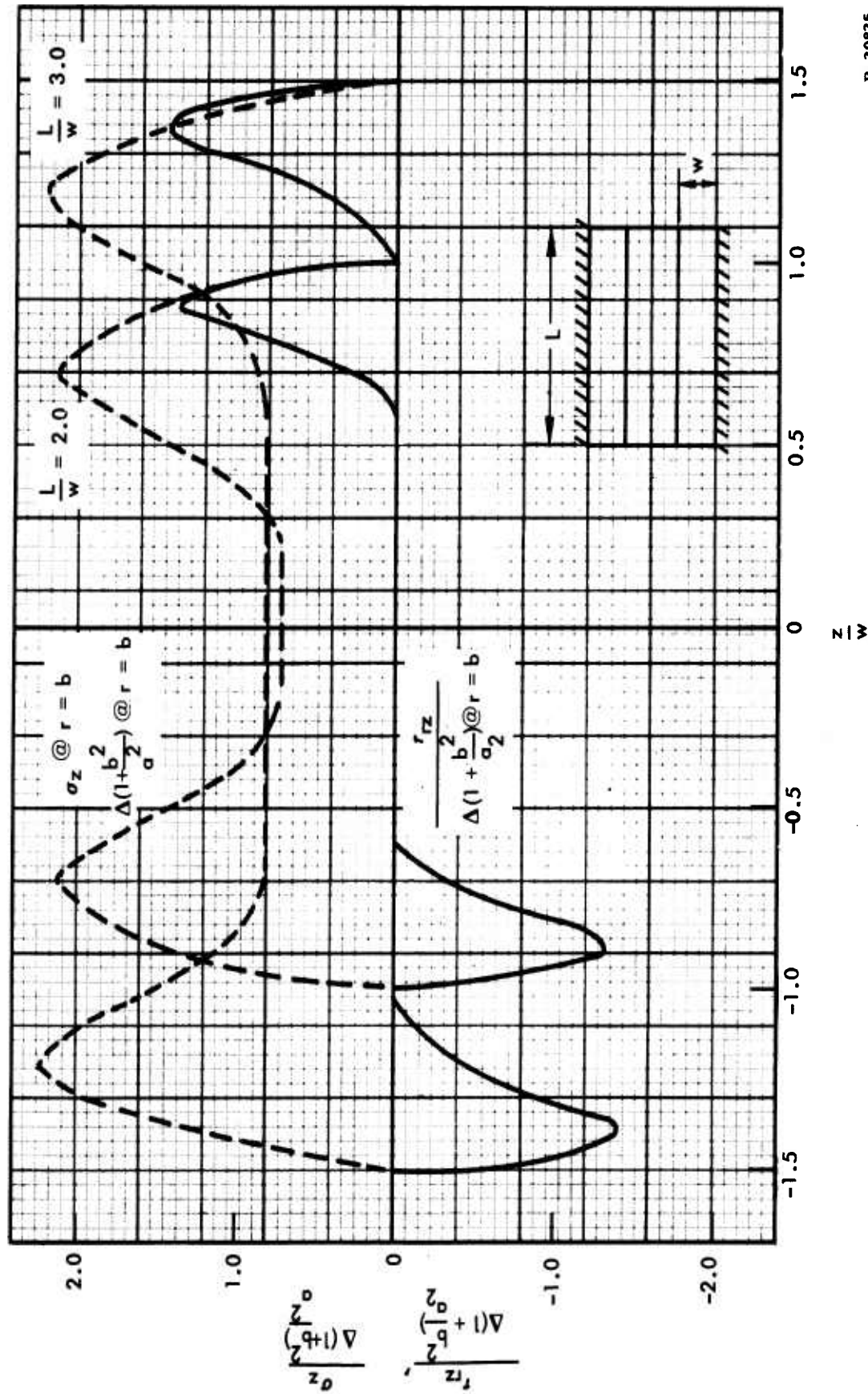
R-20825

Figure 3. Stress Due to Thermal Loads Along
a Fixed Edge — Finite Length Cylinder
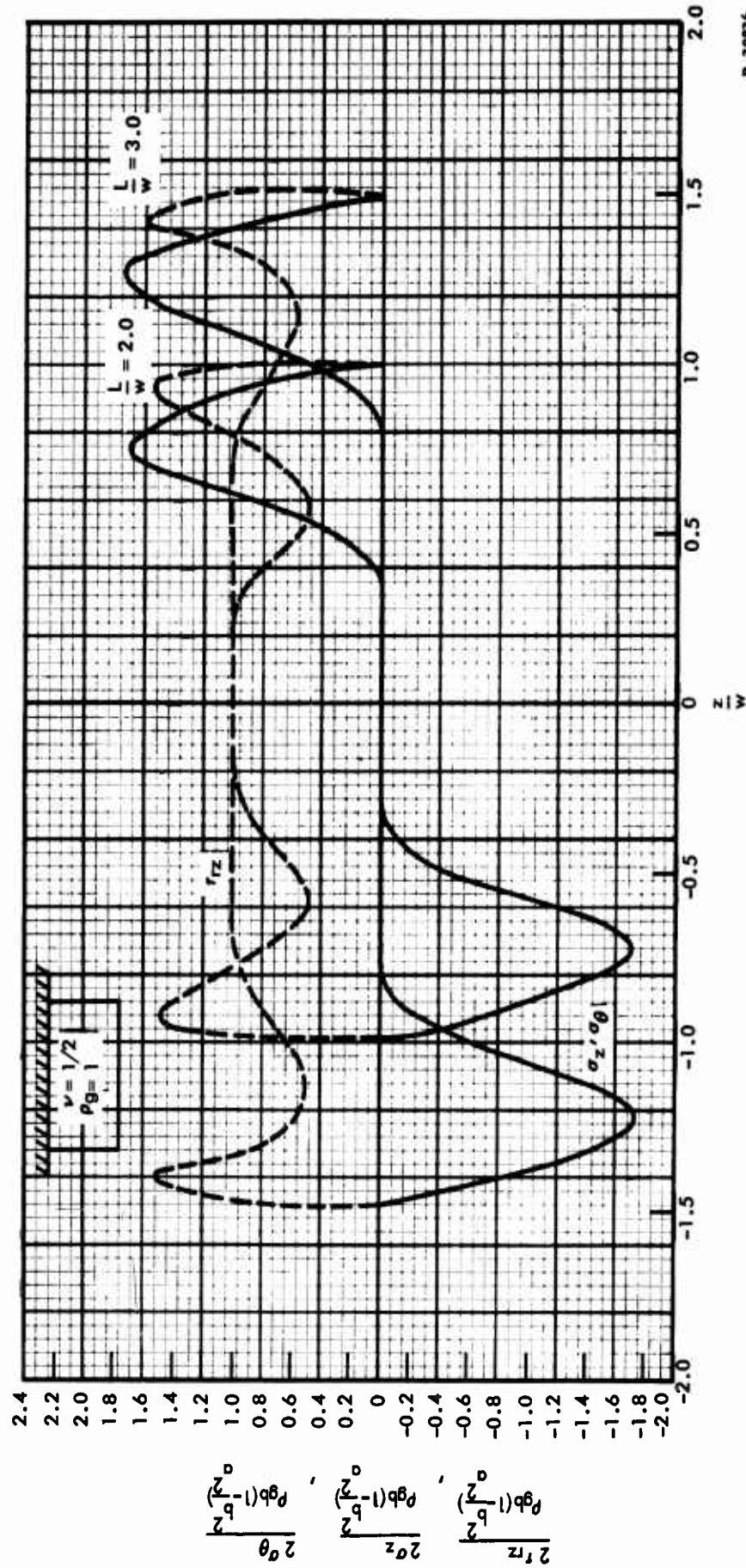
Figure 4. Stresses Due to Gravitational Loads Along a Fixed Edge —
Finite Length Cylinder

place, polymerization has occurred. The filling of the boot void reduces the reference or datum temperature for that portion of the cylinder. Thus cylic temperature variations will be referenced to the "ambient fill temperature" and not the cure temperatures. Therefore, the stresses are greatly reduced at the ends. It should be noted that the maximum stress condition has moved to the base of the boot. A case debond may occur as a result of a temperature variation at the base of the boot, and yet the ends remain crack free.

2.2.3 Stresses in a Hollow Cylinder

A cured circular cylindrical propellant grain can be idealized initially to an elastic, infinitely long, hollow cylinder bonded at its outer surface (r = b) to a steel case (Figure 5). The inner surface (r = a) is assumed

R-20827
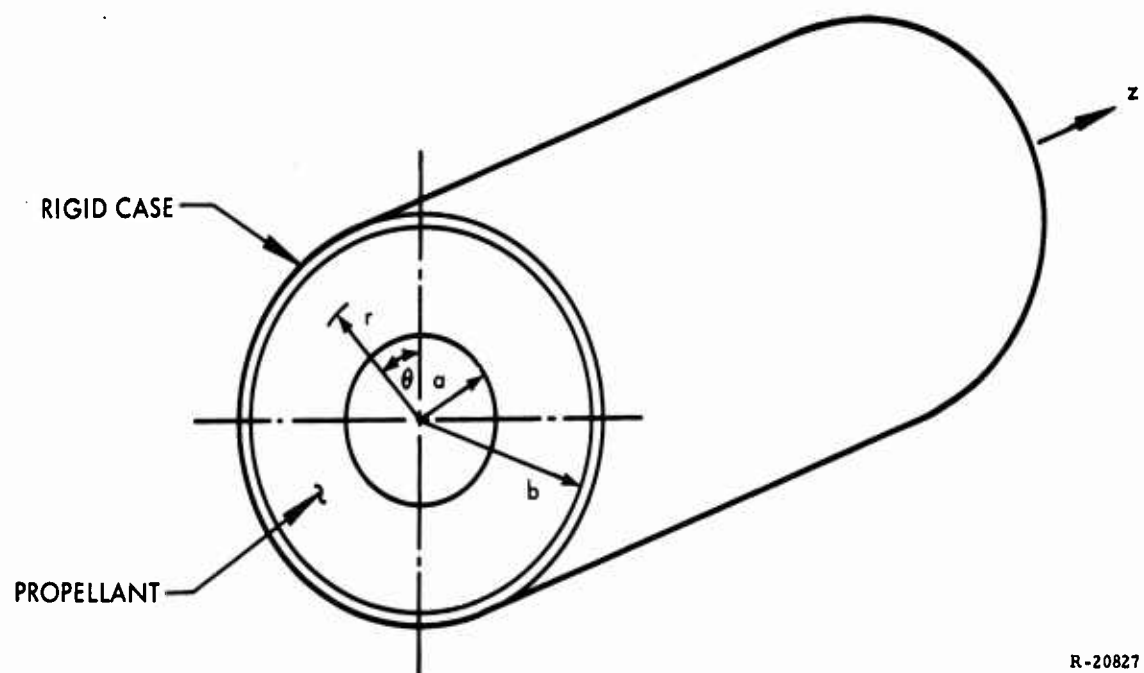
Figure 5. Grain Configuration

to be free of normal and shearing stresses. At a temperature, T ,
the cylinder is free of stress. The cylinder is assumed to be elastic
(having a modulus of elasticity, E) and obeys the Duhamel-Neumann
(Reference 8) stress-strain relations. Its coefficient of linear
expansion is α_p , while that of the steel case is α_c . The change
in volume due to polymerization of the propellant can be expressed
by the ratio $\frac{\Delta V}{V}$. The problem is to determine the maximum
stresses in the cylinder caused by the decrease in temperature from
T to $T - \Delta T$.

Due to a difference between the coefficients of linear expansion of
case and propellant, a stress distribution will arise in the propellant
grain when the temperature changes. Assuming the case to be elas-
tically rigid, the equations for the stress field of an infinitely long
cylinder can be easily obtained (Reference 9). The three normal
stresses have the form of the Lamé equations. For Poisson's ratio
$\nu = \frac{1}{2}$ (Section 2.2.4) the stresses are

$$\sigma_r = E\left[(\alpha_p - \alpha_c)\,\Delta T + \frac{\Delta V}{3\,V}\right]\left[\frac{b^2}{a^2}\right]\left[1 - \frac{a^2}{r^2}\right] \tag{11}$$

$$\sigma_\theta = E\left[(\alpha_p - \alpha_c)\,\Delta T + \frac{\Delta V}{3\,V}\right]\left[\frac{b^2}{a^2}\right]\left[1 + \frac{a^2}{r^2}\right] \tag{12}$$

$$\sigma_z = E\left[(\alpha_p - \alpha_c)\,\Delta T + \frac{\Delta V}{3\,V}\right]\left[1 + \frac{b^2}{a^2}\right] \tag{13}$$

If the cylinder is now assumed to be of finite length, the ends of the
cylinder have normal stresses in accordance with Equation 13. To
duplicate the stress condition of the propellant grain, no external
forces or stresses are applied to the ends of the hollow cylinder.

Therefore, the end surfaces must have the normal stresses described in Equation 13 removed. This is done by superposing equal and opposite normal stresses on the ends of the cylinder. This latter problem, sometimes referred to as the "reduced problem," has no known exact solution at present.

Therefore, to develop a more clear understanding to the stress distribution in the cylinder for the reduced problem, consider the case of a semi-infinite slab (Figure 6). The correspondence between the semi-infinite slab and the semi-infinitely long hollow cylinder is geometric. That is, if the radius to the centroid of the longitudinal cross sectional area of a hollow cylinder becomes infinitely large or if the ratio of the outer to inner diameters, $\frac{b}{a}$, approaches one, the hollow cylinder degenerates into the slab. At the ratio $\frac{b}{a} = 1$, the elastic stress solutions of the two bodies would also be the same.
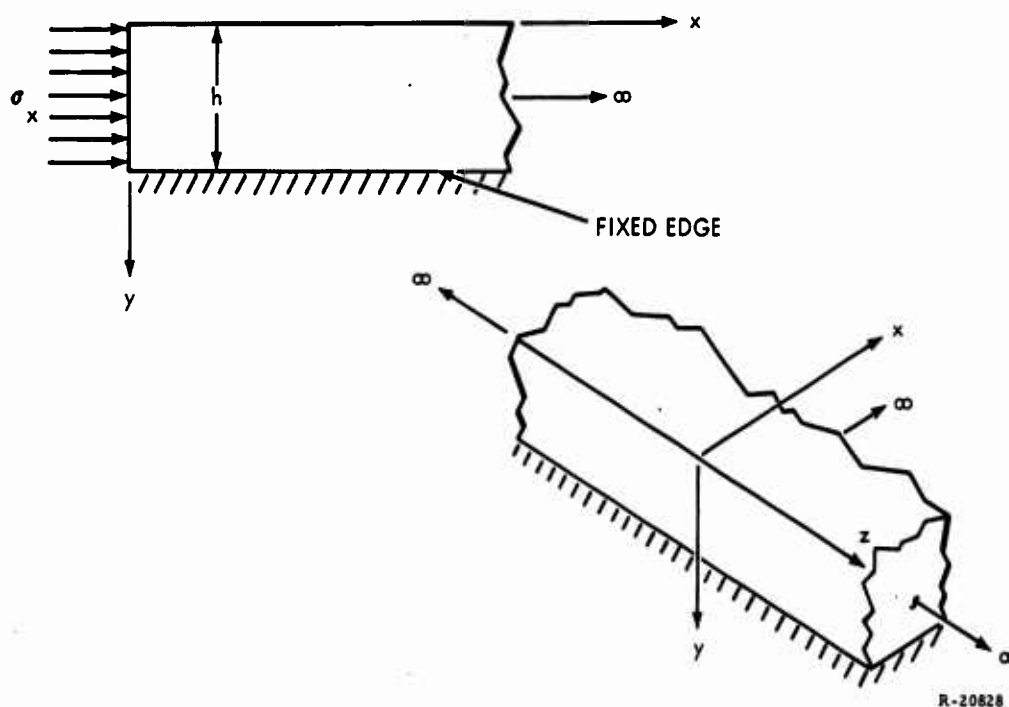
Figure 6. Semi-Infinite Slab

2.2.3.1 Stresses in a Semi-Infinite Slab (Thermal Loading)

The slab is assumed to have the same elastic characteristics as the hollow cylinder. If the slab were imagined to be free, as a result of a uniform temperature change, ΔT, the body would have strains developed

$$\epsilon_x = \epsilon_y = \epsilon_z = \alpha_p \Delta T$$

$$\epsilon_{xy} = 0 \tag{14}$$

and the steel case would have strains

$$\epsilon_x = \epsilon_y = \epsilon_z = \alpha_c \Delta T$$

$$\epsilon_{xy} = 0 \quad . \tag{15}$$

Consider plane strain to exist in the z direction. Since the relative displacement between the slab and steel casing must be zero, a stress must be developed throughout the body having one magnitude

$$\sigma_x = E_p (\alpha_p - \alpha_c) \Delta T = E \alpha \Delta T \tag{16}$$

As for the cylinder, the end surfaces must have the normal stresses described in Equation 16. To remove these stresses, equal and opposite normal stresses are superposed. Again the "reduced problem" is defined.

At the end plane $x = 0$ (Figure 6), a uniform normal stress is applied

$$\sigma_x = - E \alpha \Delta T \quad . \tag{17}$$

At the other end, or at $x = \infty$, the normal stress is assumed to be zero. All other free surfaces are free from stress.

The following method is primarily due to Aleck (Reference 10). Although his method is essentially correct, some assumptions, results, and conclusions need a critical review. Assume that the normal stress distribution in the x direction has the form

$$\sigma_x = \sum_{n=1}^{m} f_n(x) y^{n-1} \quad . \tag{18}$$

From equilibrium conditions,

$$\frac{\partial \sigma_x}{\partial x} + \frac{\partial \tau_{xy}}{\partial y} = 0 \quad . \tag{19}$$

The shearing stress can thus be expressed as

$$\frac{\partial \tau_{xy}}{\partial y} = - \sum f_n' y^{n-1} \quad , \tag{20}$$

$$\tau_{xy} = - \sum_{n=1}^{m} \frac{f_n' y^n}{n} + G_1(x) \quad . \tag{21}$$

To satisfy the boundary condition,

$$\tau_{xy}(x, 0) = 0 \quad . \tag{22}$$

Use of Equation 22 assures that the stress tensor is symmetric $(\sigma_{ij} = \sigma_{ji})$. This assumption implies first order linear theories of elasticity; therefore,

$$G_1(x) = 0 \quad . \tag{23}$$

Note, a convenient form in notation is introduced

$$f_n = f_n(x), \quad f_n' = \frac{\partial f_n}{\partial x}, \quad f_n'' = \frac{\partial^2 f_n}{\partial x^2}, \quad \text{etc.}$$

The second equilibrium condition states

$$\frac{\partial \sigma_y}{\partial x} + \frac{\partial \tau_{xy}}{\partial x} = 0 \quad . \tag{24}$$

Thus, the stress in the y direction, σ_y, can be expressed as

$$\frac{\partial \sigma_y}{\partial y} = \sum_{n=1}^{m} \frac{f_n'' y^n}{n} \tag{25}$$

or

$$\sigma_y = \sum_{n=1}^{m} \frac{f_n'' y^{n+1}}{n(n+1)} + G_2(x) \quad . \tag{26}$$

To satisfy the boundary condition,

$$\sigma_y(x, 0) = 0 \quad , \tag{27}$$

we obtain

$$G_2(x) = 0 \quad .$$

To obtain a solution for f_n, the variational approach (Reference 11) to minimize the strain energy expression is used. The complementary energy expression for plane strain has the form

$$U = \frac{1-\nu^2}{2E} \int_{x_1}^{x_2} \int_{y_1}^{y_2} \left\{ \sigma_x^2 + \sigma_y^2 - \frac{2\nu}{1-\nu} \sigma_x \sigma_y + \frac{2\tau_{xy}^2}{1-\nu} \right\} dx\,dy - \int_\Gamma \sigma_u u\,ds \tag{28}$$

The second integral is that portion of the surface of the body, Γ, over which the displacements are specified. Along the clamped edge, the displacement is specified as zero. Thus, the integrand of the second integral is zero. In addition, the remainder of the above expression can be normalized such that

$$\overline{x} = \frac{x}{h} \tag{29}$$

and

$$\overline{y} = \frac{y}{h} \quad .$$

Introducing Equations 18, 21, and 26 into Equation 28 and using the variation principle for each function, f_i, a set of differential equations will be obtained in the form

$$\delta U = \int_{x_1}^{x_2} \int_{y_1}^{y_2} \left[\frac{\partial u}{\partial f_i} - \frac{\partial}{\partial x} \left(\frac{\partial u}{\partial f_{i_x}} \right) + \frac{\partial^2}{\partial x^2} \left(\frac{\partial u}{\partial f_{i_{xx}}} \right) \right] \delta f_i \, d\overline{y} \, d\overline{x} \quad .$$

$$\text{where:} \quad (\;)_{xx} = \frac{\delta (\;)}{\delta \left(\frac{\delta^2 f}{\delta x^2} \right)} \tag{30}$$

This condition, Equation 30, is a necessary condition, insuring that the integral

$$U = \int \int F(f_1, f_2, \cdots, f_n) \, d\overline{y} \, d\overline{x} = \text{minimum} \quad . \tag{31}$$

However, imposing minimum complementary energy is not sufficient to insure that the clamped edge ($\overline{y} = 1$) conditions are maintained as necessary conditions.

For the displacement boundary condition at the fixed edge, the stress-strain relations in the $\bar{x}$ direction can be expressed as

$$E\epsilon_x = \frac{\partial u}{\partial x} = \sigma_x(1 - \nu^2) - \sigma_y \nu(1 + \nu) = 0 \quad . \qquad (32)$$

thus, a relation between the normal inplane stress components results

$$\sigma_x = \sigma_y \left(\frac{\nu}{1 - \nu}\right) \quad . \qquad (33)$$

In addition, the displacement in the y direction, v, is zero at the fixed edge. Again using stress-strain relationship,

$$E\epsilon_y = \frac{\partial \nu}{\partial y} = \sigma_y(1 - \nu^2) - \sigma_x \nu(1 + \nu) \quad . \qquad (34)$$

Substituting Equations 18 and 26 into 34 and integrating, the displacement is defined as

$$v = \sum_{n=1}^{m} \frac{f_n'' \bar{y}^{n+2}(1 - \nu^2)}{n(n+1)(n+2)} - \sum_{n=1}^{m} \frac{f_n \bar{y}^{n+1} \nu(1 + \nu)}{n+1} + V(x) , \quad (35)$$

where

$$V(x) = -\sum_{n=1}^{m} \frac{f_n''(1 - \nu^2)}{n(n+1)(n+2)} + \sum_{n=1}^{m} \frac{f_n \nu(1 + \nu)}{n+1} \quad .$$

Note that the displacement boundary condition in the y direction is satisfied identically by the function $V(x)$. The displacement in the x direction, u , or its derivative, however, as described by Equation 32, is not assured. Thus, the relationship in Equation 33 must be used as an auxiliary boundary condition (Reference 12).

Substituting Equations 18 and 26 into Equation 33, the non-holonomic condition is provided at the fixed boundary $(\overline{y} = 1)$

$$\sum_{n=1}^{m} f_n - \frac{\nu}{1-\nu} \sum_{n=1}^{m} \frac{f_n''}{n(n+1)} \cdot \tag{36}$$

or simply expressed in functional form

$$G(f_n, f_n'') = 0 \quad . \tag{37}$$

Now to insure that Equation 33 is satisfied as well as the complementary energy being a minimum, the Lagrangian multiplier, ξ, (Reference 12) is used in the variation. Thus, Equation 31 is modified, such that,

$$U^* = U + \xi G \quad . \tag{38}$$

The variation of the modified energy can be expressed as

$$\delta U^* = \delta (U + \xi G) \quad , \tag{39}$$

where

$$\xi = \xi(x) \quad .$$

The complementary energy can be determined by substituting Equations 18, 21, and 26 into 28

$$U = \int_{x_1}^{x_2} \int_{y_1}^{y_2} \left\{ \sum_{i=1}^{m} \sum_{n=1}^{m} f_i f_n \overline{y}^{n+i+2} + \sum_{i=1}^{m} \sum_{n=1}^{m} \frac{f_i'' f_n'' \overline{y}^{n+i+2}}{in(n+1)(i+1)} \right. $$
$$\left. + \frac{2}{1-\nu} \sum_{i=1}^{m} \sum_{n=1}^{m} \frac{f_i' f_n' \overline{y}^{n+i}}{in} - \frac{2\nu}{1-\nu} \sum_{i=1}^{m} \sum_{n=1}^{m} \frac{f_i f_n'' \overline{y}^{n+i}}{n(n+1)} \right\} d\overline{y} d\overline{x} \tag{40}$$

However, to introduce the subsidiary boundary conditions according to Equation 38, the following relation must hold

$$U^* = U + \int_{x_1}^{x_2} \int_{y_1}^{y_2} \xi \left\{ \sum_{n=1}^{m} f_n - \frac{\nu}{1-\nu} \sum_{n=1}^{m} \frac{f_n''}{n(n+1)} \right\} d\bar{y} d\bar{x} . \quad (41)$$

Since the functions f_n, f_i, and ξ are functions in x only, the y variable can be evaluated for $\bar{y}_1 = 0$ and $\bar{y}_2 = 1$

$$U^* = \int_{x_1}^{x_2} \left\{ \sum_{i=1}^{m} \sum_{n=1}^{m} \frac{f_i f_n}{(n+i-1)} + \sum_{i=1}^{m} \sum_{n=1}^{m} \frac{f_i'' f_n''}{i n (n+1)(i+1)(n+i+3)} \right.$$

$$+ \frac{2}{1-\nu} \sum_{i=1}^{m} \sum_{n=1}^{m} \frac{f_i' f_n'}{i n(n+i+1)} - \frac{2\nu}{1-\nu} \sum_{i=1}^{m} \sum_{n=1}^{m} \frac{f_i f_n''}{n(n+1)(n+i+1)}$$

$$+ \xi \sum_{i=1}^{m} f_n - \frac{\xi \nu}{1-\nu} \sum_{i=1}^{m} \frac{f_n''}{n(n+1)} \left. \right\} d\bar{x} . \quad (42)$$

Applying Equation 30 to 42 for each function f_i and ξ we obtain:

$$\delta U^* = \int_{x_1}^{x_2} \left\{ \sum_{i=1}^{m} \sum_{n=1}^{m} \frac{2f_n}{n+i-1} - \frac{4}{1-\nu} \sum_{i=1}^{m} \sum_{n=1}^{m} \left(\frac{1}{i n(n+i+1)} \right. \right.$$

$$+ \nu \left. \frac{i(i+1) + (n+1) n}{i n(n+1)(i+1)(i+n+1)} \right) f_n'' + \sum_{i=1}^{m} \sum_{n=1}^{m} \frac{2}{i n(n+1)(i+1)(n+i+3)} f_n^{IV}$$

$$+ \sum_{i=1}^{m} \left(\xi - \frac{\nu}{1-\nu} \frac{\xi''}{i(i+1)} \right) \left. \right\} \delta f_i d\bar{x} = 0 \quad (43)$$

It is noted that the function within the braces has the general form of the Euler-Lagrangian equation.

$$a_{in} + b_{in} f_i'' + c_{in} f_i^{IV} = 0 \qquad (44)$$

There are, however, m number of Euler equations that must be solved simultaneously,

$$\left[a_{ij} + b_{ij} D^2 + c_{ij} D^4 \right] f_i = 0 \qquad (45)$$

where

$$i, j = (1, 2, \cdots, m)$$
$$D^2 = \frac{\partial^2}{\partial x^2} \quad , \text{ etc.}$$

Solution to the previous equation is obtained by merely replacing the derivative with its characteristic root or eigenvalue, λ_i, and solving the resultant determinant (D matrix). (Refer to Reference 13.) The form of the functions is therefore

$$f_i = \sum_{n=1}^{2i} A_{in} e^{\lambda_i \overline{x}} \quad . \qquad (46)$$

As a numerical example, assume $i = 3$; the resultant D matrix would be expressed as

$$\begin{bmatrix} 2 - \left(\frac{4}{3} + 2\nu\right)\frac{D^2}{1-\nu} + \frac{D^4}{10} & , & 1 - \left(\frac{1}{2} + \frac{5\nu}{6}\right)\frac{D^2}{1-\nu} + \frac{D^4}{36} & , & \frac{2}{3} - \left(\frac{4}{15} + \frac{\nu}{2}\right)\frac{D^2}{1-\nu} + \frac{D^4}{84} & , & 1 - \frac{\nu}{2(1-\nu)} D^2 \\[2ex] 1 - \left(\frac{1}{2} + \frac{5\nu}{6}\right)\frac{D^2}{1-\nu} + \frac{D^4}{36} & , & \frac{2}{3} - \left(\frac{1}{5} + \frac{\nu}{3}\right)\frac{D^2}{1-\nu} + \frac{D^4}{126} & , & \frac{1}{2} - \left(\frac{1}{9} + \frac{14\nu}{72}\right)\frac{D^2}{1-\nu} + \frac{D^4}{288} & , & 1 - \frac{\nu}{6(1-\nu)} D^2 \\[2ex] \frac{2}{3} - \left(\frac{4}{15} + \frac{\nu}{2}\right)\frac{D^2}{1-\nu} + \frac{D^4}{84} & , & \frac{1}{2} - \left(\frac{1}{9} + \frac{14\nu}{72}\right)\frac{D^2}{1-\nu} + \frac{D^4}{288} & , & \frac{2}{5} - \left(\frac{4}{63} + \frac{\nu}{9}\right)\frac{D^2}{1-\nu} + \frac{D^4}{648} & , & 1 - \frac{\nu}{12(1-\nu)} D^2 \\[2ex] 1 - \frac{\nu}{2(1-\nu)} D^2 & , & 1 - \frac{\nu}{6(1-\nu)} D^2 & , & 1 - \frac{\nu}{12(1-\nu)} D^2 & , & 0 \end{bmatrix} \begin{bmatrix} f_1 \\[2ex] f_2 \\[2ex] f_3 \\[2ex] \xi \end{bmatrix} = 0 \qquad (47)$$

Thus, the form of the functions, f_i and ξ, can be expressed as

$$f_1 = \sum_{i=1}^{6} A_{1i} \, e^{\lambda_i x}$$

$$f_2 = \sum_{i=1}^{6} B_{1i} \, e^{\lambda_i x}$$

$$f_3 = \sum_{i=1}^{6} C_{1i} \, e^{\lambda_i x} \tag{48}$$

$$\xi = \sum_{i=1}^{6} D_{1i} \, e^{\lambda_i x}$$

For convenience, a Poisson's ratio of 1/2 will be assumed as a sample of this procedure since it is representative for most solid propellants. The eigenvalues are listed in Table I.

TABLE I

EIGENVALUES OF EQUATION 47

$$\lambda_1 \quad = \quad -0.69357712$$
$$\lambda_{2,3} \quad = \quad -1.7043982 \pm i\,2.849476$$
$$\lambda_{4,5} \quad = \quad -3.5030151 \pm i\,6.7263859$$
$$\lambda_6 \quad = \quad -14.030111$$

Since the eigenvalue, λ, is a root of the determinant, so is its conjugate, $\bar{\lambda}$, as well as their negatives. Since Equation 46 is of the exponential form, a decaying or negative eigenvalue will therefore be used. Thus, the upper limit of the summation on f_i is twice the number of functions chosen.

By substituting Equations 48 into Equation 47, moving the first column matrix of Equation 45, A_{ij}, to the right hand side of the equation, and using $n - 1$, homogeneous equations, the ratio for each element in the matrix $(B/A)_i$, and $(D/A)_i$ is obtained

$$\begin{bmatrix} B/A \\ C/A \\ D/A \end{bmatrix}_i = \begin{bmatrix} B_{11} & C_{11} & D_{11} \\ B_{21} & C_{21} & D_{21} \\ B_{31} & C_{31} & D_{31} \end{bmatrix}^{-1} \cdot \begin{bmatrix} A_{11} \\ A_{21} \\ A_{31} \end{bmatrix} \qquad (49)$$

The axial stress at $x = 0$ is normalized so that $\sigma_x = \alpha\, ET = 1$ and $\tau_{xy} = 0$.

In satisfying the remaining boundary conditions, therefore, the following equations must be satisfied:

$$\left\{ \begin{array}{ll} \displaystyle\sum_{i=1}^{6} A_i = 1 & \displaystyle\sum_{i=1}^{6} \lambda_i A_i = 0 \\[2em] \displaystyle\sum_{i=1}^{6} B_i = 0 & \displaystyle\sum_{i=1}^{6} \lambda_i B_i = 0 \\[2em] \displaystyle\sum_{i=1}^{6} C_i = 0 & \displaystyle\sum_{i=1}^{6} \lambda_i C_i = 0 \end{array} \right\} \qquad (50)$$

or substituting values from Equation 49

$$
\begin{bmatrix}
1 & 1 & 1 & 1 & 1 & 1 \\
(B/A)_1 & (B/A)_2 & (B/A)_3 & (B/A)_4 & (B/A)_5 & (B/A)_6 \\
(C/A)_1 & (C/A)_2 & (C/A)_3 & (C/A)_4 & (C/A)_5 & (C/A)_6 \\
\lambda_1 & \lambda_2 & \lambda_3 & \lambda_4 & \lambda_5 & \lambda_6 \\
(\lambda \frac{B}{A})_1 & (\lambda \frac{B}{A})_2 & (\lambda \frac{B}{A})_3 & (\lambda \frac{B}{A})_4 & (\lambda \frac{B}{A})_5 & (\lambda \frac{B}{A})_6 \\
(\lambda \frac{C}{A})_1 & (\lambda \frac{C}{A})_2 & (\lambda \frac{C}{A})_3 & (\lambda \frac{C}{A})_4 & (\lambda \frac{C}{A})_5 & (\lambda \frac{C}{A})_6
\end{bmatrix}
\begin{bmatrix}
A_1 \\ A_2 \\ A_3 \\ A_4 \\ A_5 \\ A_6
\end{bmatrix}
=
\begin{bmatrix}
1 \\ 0 \\ 0 \\ 0 \\ 0 \\ 0
\end{bmatrix}
\qquad (51)
$$

The values of the coefficients are summarized in Table II.

TABLE II

SOLUTION VECTOR OF EQUATION 51

$$A_1 = 1.4737285$$

$$A_{2,3} = -0.60773211 \pm i\ 0.45652196$$

$$A_{4,5} = 0.60715210 \pm i\ 0.44805945$$

$$A_6 = -0.47256973$$

By substituting the coefficients from Table II into Equation 48 and into Equations 18, 21, and 26, the stresses along the fixed edge are obtained (Figure 7). To obtain the final stress distribution along the wall, Equation 16 must be added to Equation 18. This is represented in Figure 8.
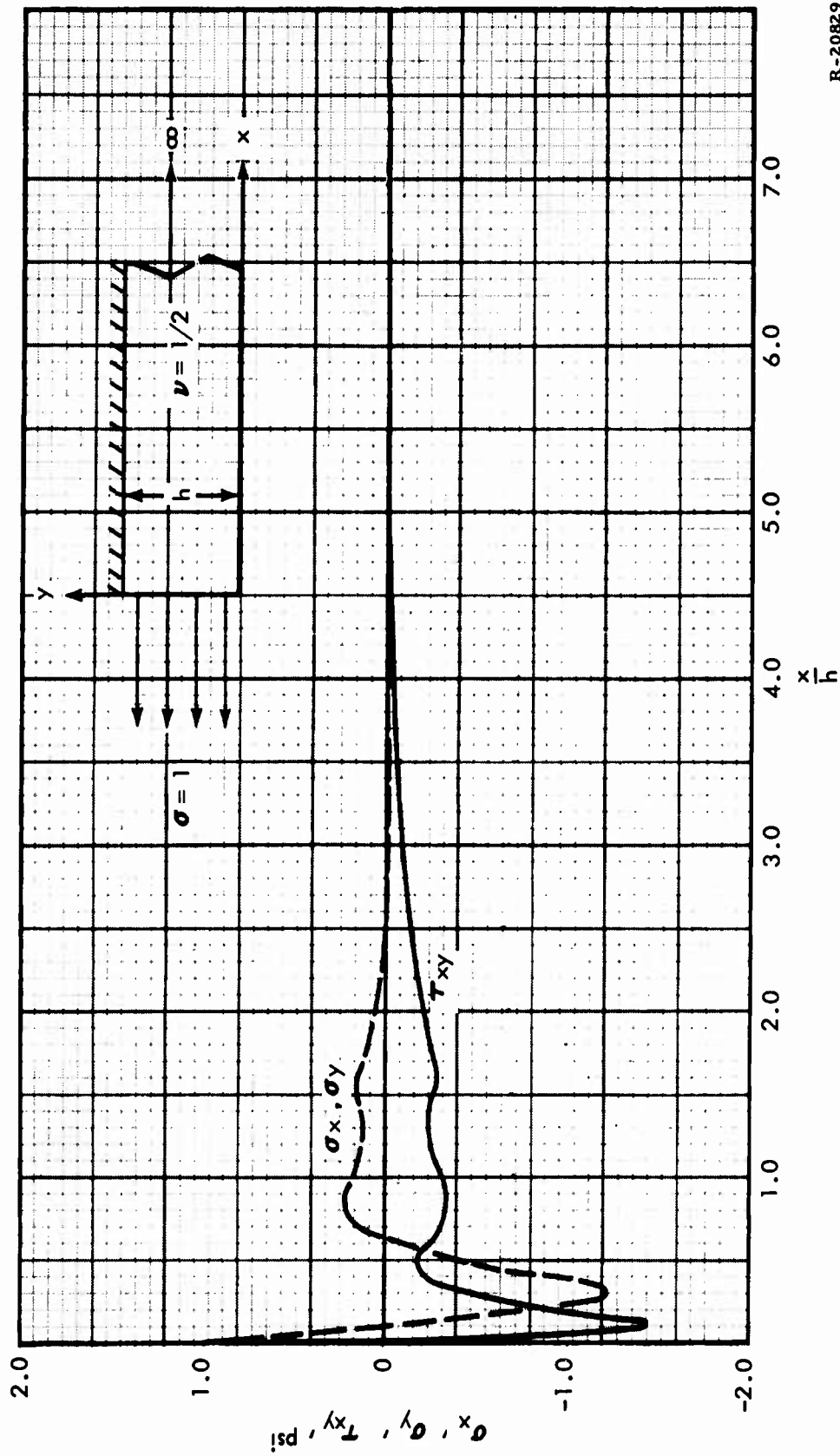
Figure 7. Stresses Along a Fixed Edge for Reduced Problem

R-20829
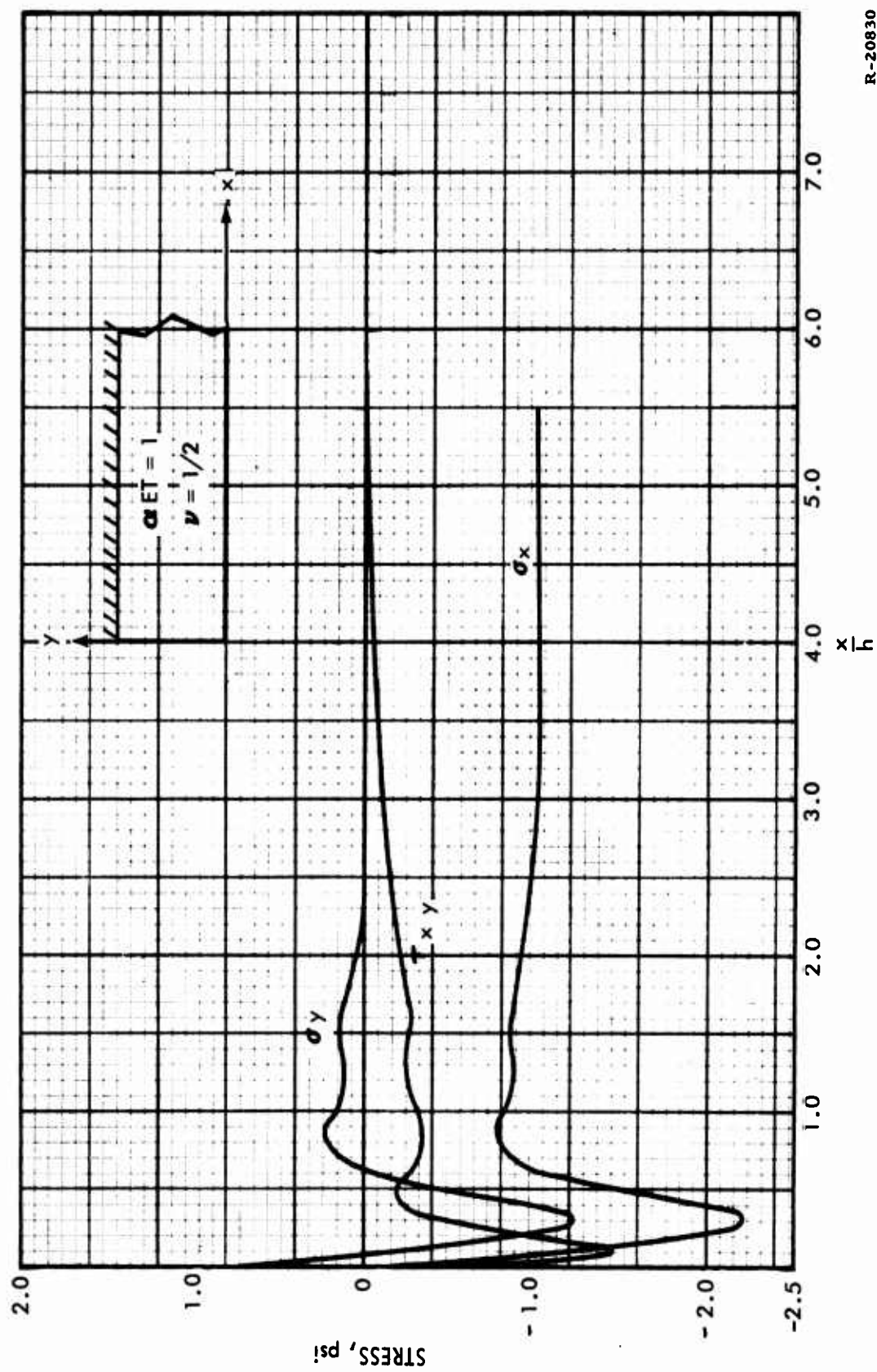
Figure 8. Stresses Along a Fixed Edge for Thermal Loading

R-20830

2.2.3.2 Stresses in a Semi-Infinite Slab (Body Forces)

The second consideration is that of the stresses induced by gravitational body forces. The stresses in a vertical-standing, hollow, infinitely long cylinder, as in Figure 5, can again be easily determined (Reference 1).

$$\left.\begin{array}{l} \tau_{rz} = \dfrac{\rho g}{2}\, r \left[1 - \left(\dfrac{a}{r}\right)^2 \right] \\[2ex] \sigma_r = \sigma_z = \sigma_\theta = 0 \end{array}\right\} \tag{52}$$

All boundary conditions are satisfied except for the ends. Again, the plane strain solution of a semi-infinite slab will be considered. The expression for the maximum shearing stresses can be readily found to have the form

$$\tau_{xy} = \rho g y \quad . \tag{53}$$

From Equation 21, it is obvious that the same eigenvalues of Equation 47 can be used and only Equations 50 and 51 will change.

To satisfy the boundary condition, the following equations must be satisfied; this time the shear stress $\tau_{xy} = \rho g h = 1$ is normalized at the fixed boundary $(\overline{y} = 1)$

$$\begin{array}{ll} \displaystyle\sum_{i=1}^{6} A_i = 0 & \displaystyle\sum_{i=1}^{6} A_i \lambda_i = 1 \\[3ex] \displaystyle\sum_{i=1}^{6} B_i = 0 & \displaystyle\sum_{i=1}^{6} B_i \lambda_i = 0 \\[3ex] \displaystyle\sum_{i=1}^{6} C_i = 0 & \displaystyle\sum_{i=1}^{6} C_i \lambda_i = 0 \end{array} \tag{54}$$

Substituting values, as related in Equation 52, into Equation 54:

$$
\begin{bmatrix}
1 & 1 & 1 & 1 & 1 & 1 \\
(B/A)_1 & (B/A)_2 & (B/A)_3 & (B/A)_4 & (B/A)_5 & (B/A)_6 \\
(C/A)_1 & (C/A)_2 & (C/A)_3 & (C/A)_4 & (C/A)_5 & (C/A)_6 \\
\lambda_1 & \lambda_2 & \lambda_3 & \lambda_4 & \lambda_5 & \lambda_6 \\
(\lambda\frac{B}{A})_1 & (\lambda\frac{B}{A})_2 & (\lambda\frac{B}{A})_3 & (\lambda\frac{B}{A})_4 & (\lambda\frac{B}{A})_5 & (\lambda\frac{B}{A})_6 \\
(\lambda\frac{C}{A})_1 & (\lambda\frac{C}{A})_2 & (\lambda\frac{C}{A})_3 & (\lambda\frac{C}{A})_4 & (\lambda\frac{C}{A})_5 & (\lambda\frac{C}{A})_6
\end{bmatrix}
\begin{bmatrix}
A_1 \\ A_2 \\ A_3 \\ A_4 \\ A_5 \\ A_6
\end{bmatrix}
=
\begin{bmatrix}
0 \\ 0 \\ 0 \\ 1 \\ 0 \\ 0
\end{bmatrix}
\tag{55}
$$

The values of the coefficients are summarized in Table III.

TABLE III

SOLUTION VECTOR OF EQUATION 55

$A_1 \;=\; 2.7651613$

$A_{2,3} \;=\; 0.43679095 \;\pm\; i\; 0.70784614$

$A_{4,5} \;=\; 0.57126581 \;\pm\; i\; 0.59331908$

$A_6 \;=\; -0.54546726$

Substituting the coefficients from Table III into Equations 18, 21, and 26, the stresses along the fixed edge can be obtained, (Figure 9). Adding Equation 53 to the results from Figure 9, the final stresses along the fixed edge can be found, as represented by Figure 10.
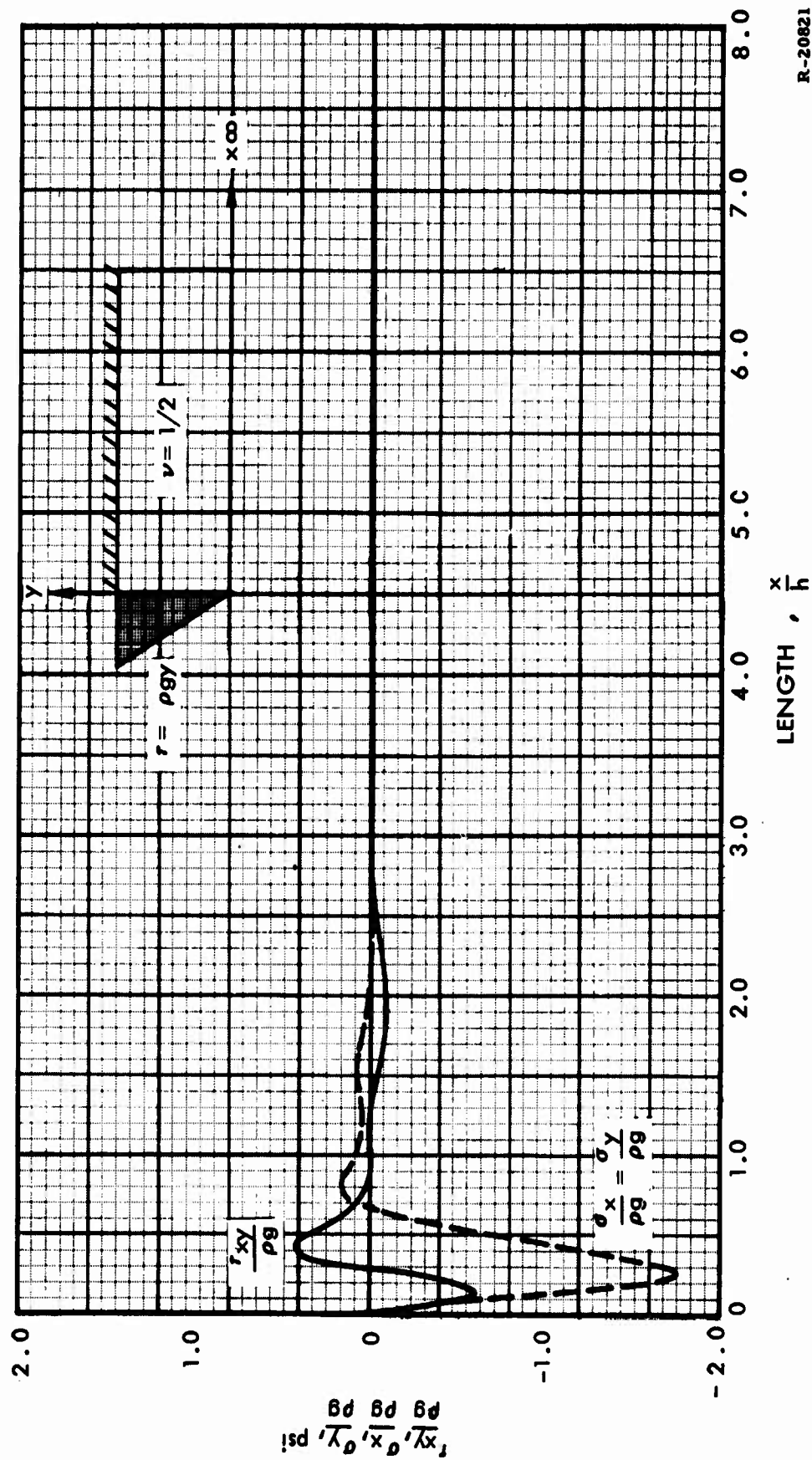
Figure 9. Stresses Along a Fixed Edge for Reduced Problem

R-20821

Figure 10. Stresses Along A Fixed Edge for Gravitational Loading

2.2.3.3 Stresses at the Re-Entrant Corner

As an alternate check, the solution for the stresses at the point $(r, z) = (b, o)$, for the hollow cylinder, may be obtained directly without solving the complete problem and without resorting to the variational method just described. The pertinent boundary conditions for the cylinder under thermal loading are

$$\sigma_r(a, o) = 0$$

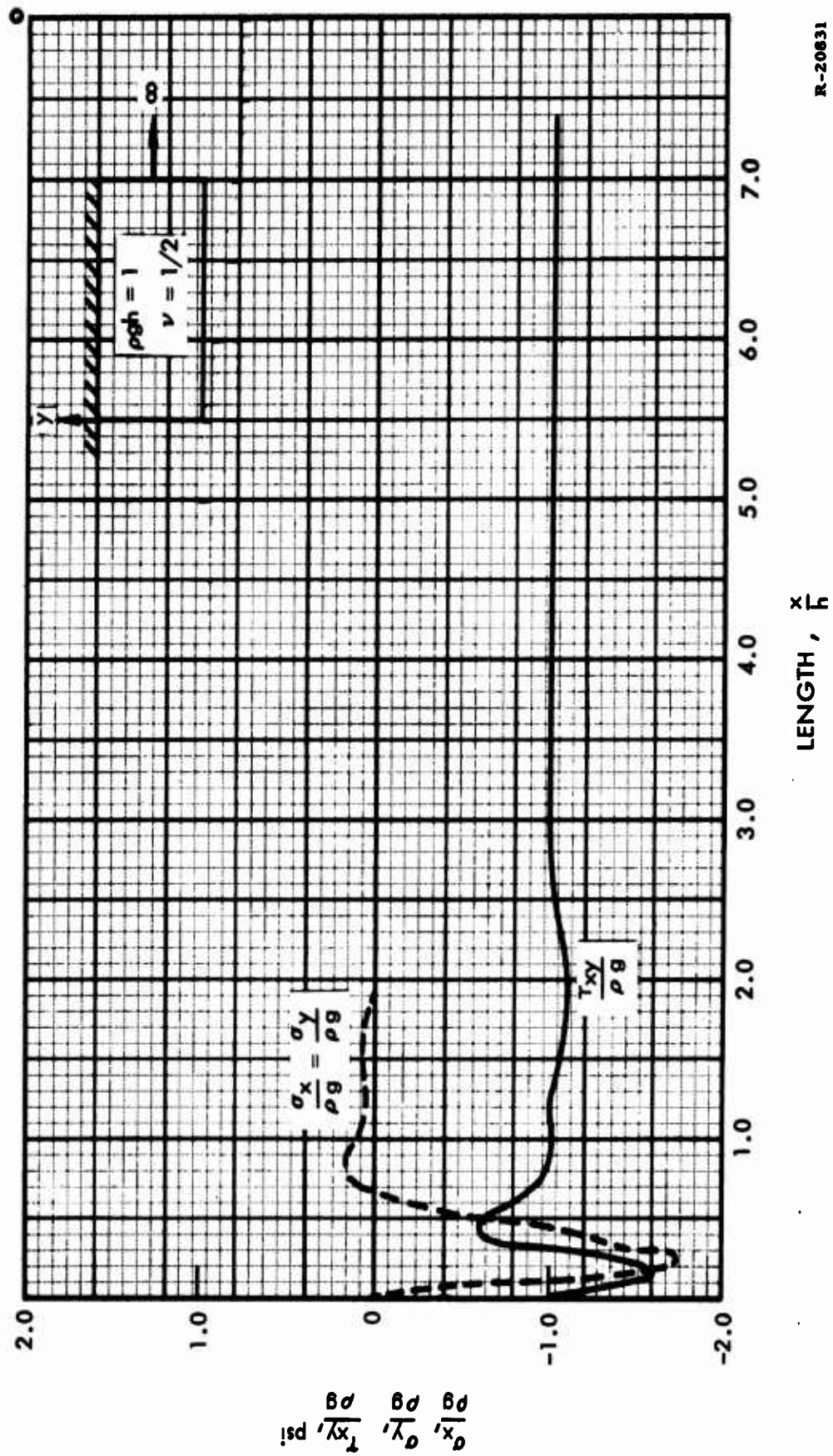$$\sigma_z(r, o) = 0 \qquad\qquad (56)$$

$$\tau_{rz}(r, o) = 0 \qquad .$$

By the Duhamel-Neumann stress-strain relations

$$\sigma_\theta = \nu(\sigma_z + \sigma_r) - E_p \, a_p \, \Delta T + E_p \, \epsilon_\theta$$

$$\qquad\qquad (57)$$

$$\sigma_z = \nu(\sigma_r + \sigma_\theta) - E_p \, a_p \, \Delta T + E_p \, \epsilon_z \qquad .$$

Eliminating σ_r from the above equation, σ_θ is obtained

$$\sigma_\theta = \sigma_z + \frac{E_p (\epsilon_\theta - \epsilon_z)}{1 - \nu} \qquad . \qquad (58)$$

Eliminating σ_θ from Eqatuion 57, σ_r is obtained:

$$\sigma_r = \frac{1 - \nu}{\nu} \sigma_z + \frac{E_p \, a_p \, \Delta T}{\nu} - \frac{E_p}{\nu(1 + \nu)} (\epsilon_\theta \nu + \epsilon_z) \qquad . \qquad (59)$$

Since the cylinder will experience equal strains due to the thermal expansion of the elastically rigid boundary and can be expressed as

$$\epsilon_\theta = \epsilon_z = a_c \Delta T \qquad , \qquad\qquad (60)$$

Equation 59 can be rewritten in the form

$$\sigma_r = \frac{1-\nu}{\nu}\,\sigma_z + \frac{E_p}{\nu}\,(\alpha_p - \alpha_c)\,\Delta T \quad . \qquad (61)$$

The stresses at the end of the cylinder can then be evaluated by introducing Equations 56 into 61,

and

$$\sigma_r = \frac{E_p\,(\alpha_p - \alpha_c)\,\Delta T}{\nu} \qquad (62)$$

$$\sigma_\theta = 0 \quad . \qquad (63)$$

If the plane strain solution is considered for $\nu = \frac{1}{2}$, Equation 61 can be written as

$$\sigma_r = \sigma_z + 2E_p(\alpha_p - \alpha_c)\,\Delta T \quad . \qquad (64)$$

From Equation 13, neglecting $\frac{\Delta V}{3V}$, the radial is expressed as

$$\sigma_r = -E_p(\alpha_p - \alpha_c)\,\Delta T \left[1 + (\frac{b}{a})^2\right] + 2E_p(\alpha_p - \alpha_c)\,\Delta T$$

$$\qquad\qquad (65)$$

$$= -E_p(\alpha_p - \alpha_c)\,\Delta T \left[(\frac{b}{a})^2 - 1\right]$$

which corresponds to Equation 11 evaluated at $r = b$.

From Equation 34 of the semi-infinite slab solution and Equation 65 of the cylindrical, reduced problem, i.e., $\sigma_z(b,o)$, is expressed by Equation 13, the two equations are of the same form. The radial component, r, corresponds to the y direction, and the axial component, z, corresponds to the x direction of the earlier problem. Thus, at the one point $(r,z) = (b,o)$ or $(x,y) = (0,1)$, the solution considering plane strain corresponds exactly to the axially symmetric solution.

Page 35

The remaining question to answer is whether the plane-strain solution for other points in the semi-infinite slab can be an analogous solution for the cylinder. Goodier (Reference 14) pointed out that, within the neighborhood of a boundary, the field equations of elasticity in cylindrical coordinates for axially symmetrical stress systems reduce to the field equations of plane strain. (A separate proof of this is presented in Section 2.2.5.) When all values of r, for the entire body, are large, this statement can be extended for the entire section. The stress distribution is analogous to the plane strain solution, provided the same boundary conditions exist. Therefore, this analogy can be extended to a cylinder of finite length, b, and the corresponding solution of an infinite strip of length, b.

2.2.3.4 Effect of Length

The length of the infinite strip can be taken into account by simply replacing f_i in Equation 46 with assumed expressions

$$f_i = \sum_{i=1}^{6} A_i' \cosh \lambda_i x$$

$$f_2 = \sum_{i=1}^{6} B_i' \cosh \lambda_i x$$

$$(66)$$

$$f_3 = \sum_{i=1}^{6} C_i' \cosh \lambda_i x$$

$$\xi = \sum_{i=1}^{6} D_i' \cosh \lambda_i x$$

This form can be assumed since it is also a solution to the Euler-Lagrangian equation as discussed in Section 2.2.3.1. Thus, the reference coordinate system is changed to the center of the body.

Substituting Equations 66 into 18, the stresses in the x direction can be determined and referenced to the center of the body. The same can also be done for the shear stresses, using Equation 21. To satisfy the boundary conditions, the following must be true:

$$
\begin{bmatrix}
\cosh \lambda_1 \frac{b}{2} & \cdots & \cosh \lambda_i \frac{b}{2} & \cdots & \cosh \lambda_m \frac{b}{2} \\
\left(\frac{B}{A}\right)_1 \cosh \lambda_1 \frac{b}{2} & \cdots & \left(\frac{B}{A}\right)_i \cosh \lambda_i \frac{b}{2} & \cdots & \left(\frac{B}{A}\right)_m \cosh \lambda_m \frac{b}{2} \\
\vdots & & \vdots & & \vdots \\
\left(\frac{m}{A}\right)_1 \cosh \lambda_1 \frac{b}{2} & \cdots & \left(\frac{m}{A}\right)_i \cosh \lambda_i \frac{b}{2} & \cdots & \left(\frac{m}{A}\right)_m \cosh \lambda_m \frac{b}{2} \\
\lambda_1 \sinh \lambda_1 \frac{b}{2} & \cdots & \lambda_i \sinh \lambda_i \frac{b}{2} & \cdots & \lambda_m \sinh \lambda_m \frac{b}{2} \\
\lambda_1 \left(\frac{B}{A}\right)_1 \sinh \lambda_1 \frac{b}{2} & \cdots & \lambda_i \left(\frac{B}{A}\right)_i \sinh \lambda_i \frac{b}{2} & \cdots & \lambda_m \left(\frac{B}{A}\right)_m \sinh \lambda_m \frac{b}{2} \\
\vdots & & \vdots & & \vdots \\
\lambda_1 \left(\frac{m}{A}\right)_1 \sinh \lambda_1 \frac{b}{2} & \cdots & \lambda_i \left(\frac{m}{A}\right)_i \sinh \lambda_i \frac{b}{2} & \cdots & \lambda_m \left(\frac{m}{A}\right)_m \sinh \lambda_m \frac{b}{2}
\end{bmatrix}
\begin{bmatrix}
A_1 \\ A_2 \\ \vdots \\ A_i \\ \vdots \\ \\ \\ A_m
\end{bmatrix}
=
\begin{bmatrix}
1 \\ 0 \\ \vdots \\ \vdots \\ \vdots \\ \vdots \\ \vdots \\ 0
\end{bmatrix}
\tag{67}
$$

Thus, substituting the above Equation 67 into Equations 18, 21, and 26, for $b = 1$ and $\nu = \frac{1}{2}$, the stresses are obtained along the fixed edge (Figure 11). Employing the same methods for the gravity loading, the stresses along the fixed edges may be obtained (Figure 12).

2.2.3.5 Discussion

Although the plane strain solution is basically two dimensional for the slab, the results are analogous to the hollow cylinder. Maintaining plane strain throughout the semi-infinite slab assures that
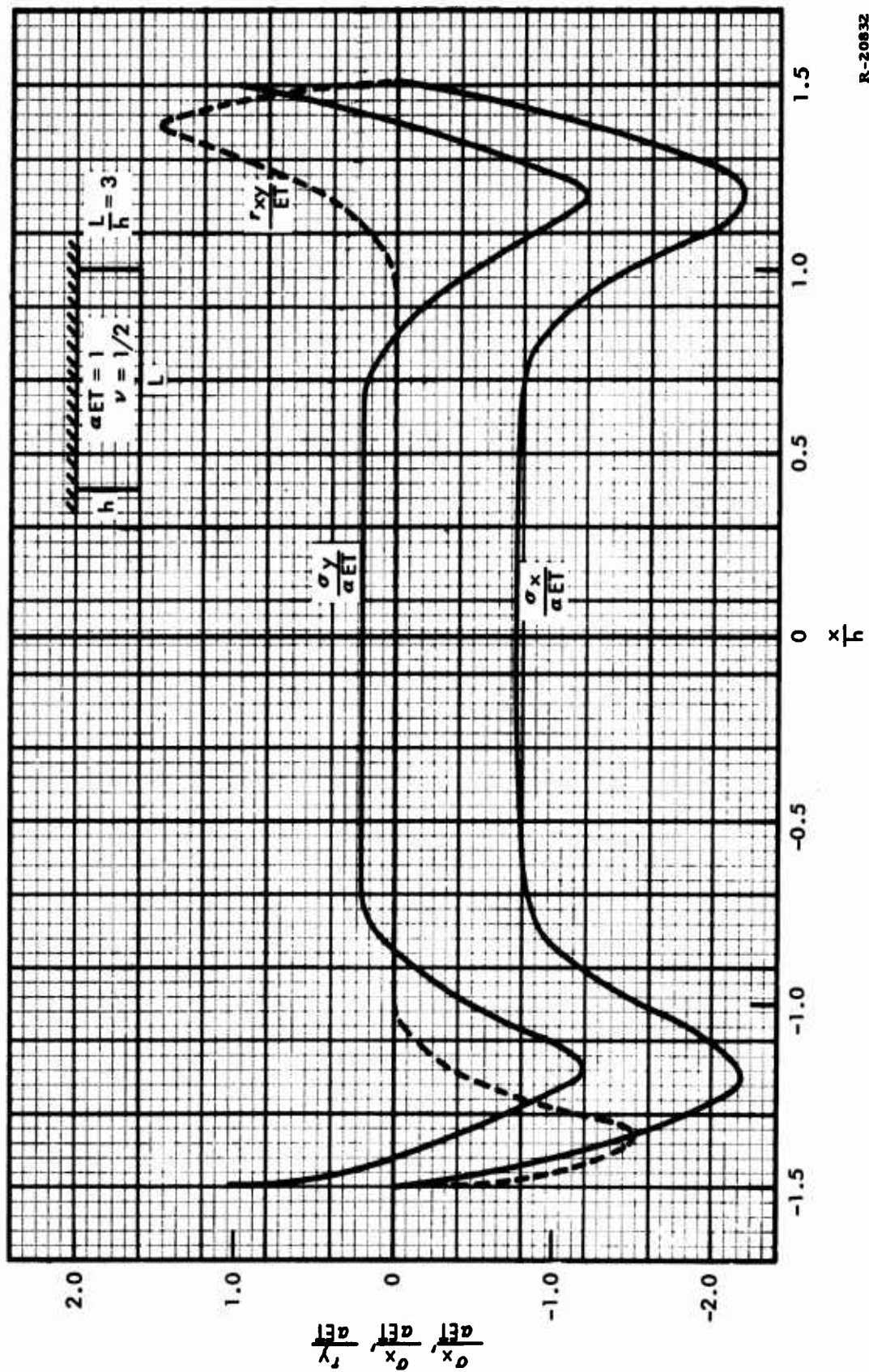
R-2032

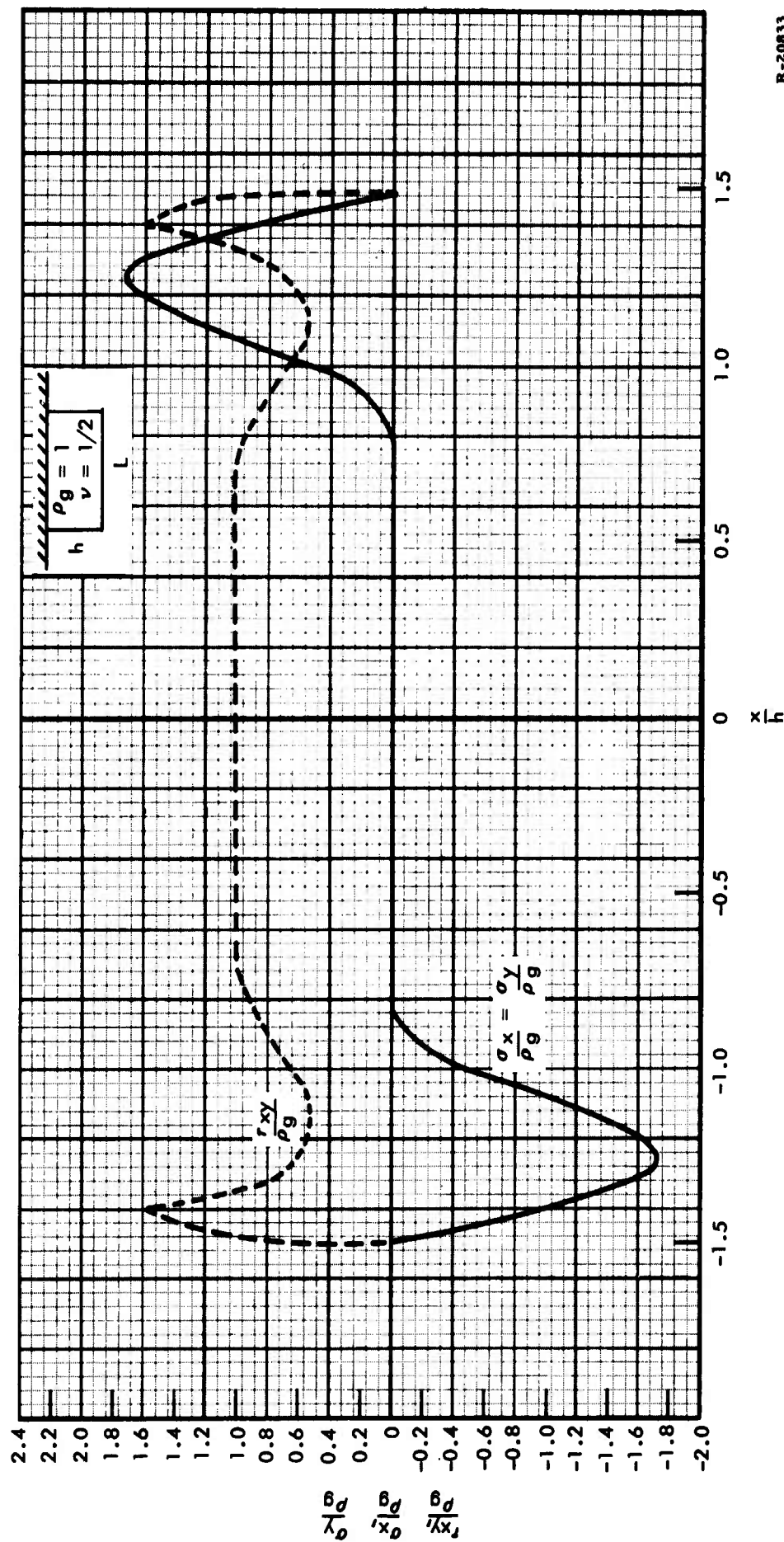Figure 11. Stresses Along a Fixed Edge for Thermal Loading — Finite Length

Figure 12.   Stresses Along a Fixed Edge for Gravitational Loading — Finite Length

a relationship exists among the stress components. Since compatibility conditions must hold, a stress reversal of the normal stress, σ_y, at the end is required. The form of the stresses is

$$\sigma = \sum_{n=1}^{\infty} A_n e^{\lambda n x} \cdot f_n(y) \tag{68}$$

The form is similar to that predicted by Horvay (Reference 15) and Kent (Reference 16). Two experimental investigations, Durelli and Tsao (Reference 17), and Zandman, Post and Redner (Reference 18), also show that the experimentally derived stresses can be represented by the same form as Equation 68.

The comparison of the predicted results to Zandman's experimental results cannot be applied directly, since the Poisson's ratio of the birefringent plastic was not reported. The principal stress difference at the corner is reported to be

$$\sigma_1 - \sigma_2 \bigg|_{\frac{x}{h}=0} = 3.0 \tag{69}$$

From previous analysis, Equation 33, the relationship of the principal stresses is satisfied only if $\nu = \frac{1}{4}$. In order to make a comparison, it is assumed that the plastic material has a Poisson's ratio, ν, of $\frac{1}{4}$.

The principal stress difference function (Figure 13) follows quite closely to the experimental results obtained by Zandman. However, the principal direction, Φ, is off as much as 20 degrees. Some
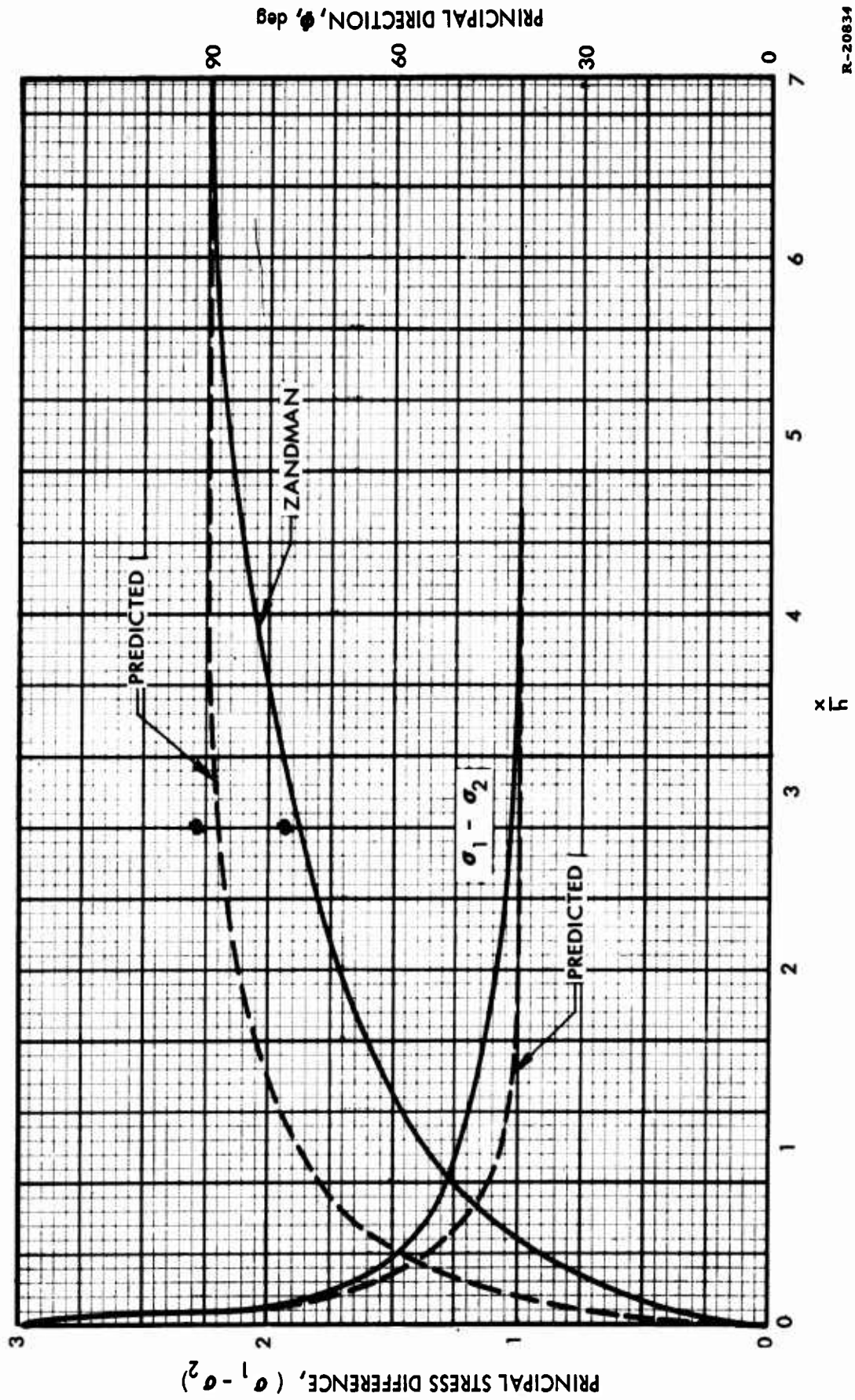
Figure 13. Comparison of Thermal Stresses Along a Fixed Edge

R-20834

of the principal factors that may alter the magnitudes of the direction function are:

1. The actual displacement boundary condition at the interface is not rigorously held. The principal cause being that the bonding agent is not infinitely rigid.

2. It is difficult to measure the isoclinics near the corner and along a fixed edge.

3. Relaxation of the stress within the material due to viscoelastic properties causes a difference in stress magnitudes.

4. The function f(y) may have a greater number of terms (i.e., order of the function being greater than three).

5. Poisson's ratio of the plastic is other than $\frac{1}{4}$.

From the theoretical standpoint, Horvay (Reference 15) and Williams (Reference 19) present the argument that a stress singularity exists at the re-entrant corner and therefore the shear stresses are infinite. Mesner (Reference 7) agrees with this argument. For two of the arguments (References 15 and 19), an initial assumption of the form of stress function causes the stress singularity. The above procedures appear to be correct, but do not agree with experimental fact. From numerical studies (References 5 and 7), the same prediction of high stresses results. Near the re-entrant corner, the numerical solution to the biharmonic equation, with mixed boundary conditions, becomes very sensitive to small changes. Thus, numerical accuracies in the method of solution may not provide adequate bounds on the iteration procedures. This, in turn, reflects itself throughout the remainder of the body, causing other boundary conditions not to be satisfied.

2.2.3.6 Conclusions

The following conclusions may be drawn from the investigation presented in Section 2.2.3:

1. The end effects problem in a hollow cylinder, at present, does not have a know exact solution.

2. The semi-infinite slab analog of the end effects problem has a solution.

3. The variational energy methods alone do not provide a strong enough condition to insure that all the boundary conditions are met. Boundary conditions are met, however, when the Lagrangian multiplier is used in conjunction with complementary energy methods.

2.2.4. The Lamé Solution

For an infinitely long, hollow cylinder bonded to an elastically rigid case, the stress-strain relations are

$$
\begin{bmatrix} \epsilon_r \\ \epsilon_\theta \\ \epsilon_z \end{bmatrix} = \frac{1}{E} \begin{bmatrix} 1 & -\nu & -\nu \\ -\nu & 1 & -\nu \\ -\nu & -\nu & 1 \end{bmatrix} \begin{bmatrix} \sigma_r \\ \sigma_\theta \\ \sigma_z \end{bmatrix} + \left[a_p \, \Delta T + \frac{1}{3} \frac{\Delta V}{V} \right] \tag{70}
$$

and have a value at the bond radius (r=b) interface of

$$
\begin{bmatrix} \epsilon_r \\ \epsilon_\theta \\ \epsilon_z \end{bmatrix} = a \, \Delta T + \frac{1}{3} \frac{\Delta V}{V} \quad . \tag{71}
$$

From equilibrium conditions with no body forces

$$
\frac{\partial}{\partial r} \left[r \, \sigma_r \right] - \sigma_\theta = 0 \tag{72}
$$

and knowing that

$$
\epsilon_r = \frac{\partial u}{\partial r} \tag{73}
$$

and

$$\epsilon_\theta = \frac{u}{r} \quad , \tag{74}$$

with the added restriction that

$$\sigma_r = 0 \Big|_{r=a} \quad ,$$

the stresses for $\nu = \frac{1}{2}$, are then found to be

$$\sigma_r = \frac{P_o \left(1 - \dfrac{a^2}{r^2}\right)}{\left(1 - \dfrac{a^2}{b^2}\right)} \tag{75}$$

and

$$\sigma_\theta = \frac{P_o \left(1 + \dfrac{a^2}{r^2}\right)}{1 - \dfrac{a^2}{b^2}} \quad , \tag{76}$$

where

$$P_o = E \left[(\alpha_p - \alpha_c) \Delta T + \frac{1}{3} \frac{\Delta V}{V} \right] \left[\frac{b^2}{a^2} - 1 \right] \quad .$$

From Equations 70, 75, and 76,

$$\sigma_z = \frac{P_o \left[1 + \dfrac{b^2}{a^2} \right]}{\left(\dfrac{b^2}{a^2} - 1 \right)} \quad . \tag{77}$$

2.2.5 Coordinate Transformation Correspondence

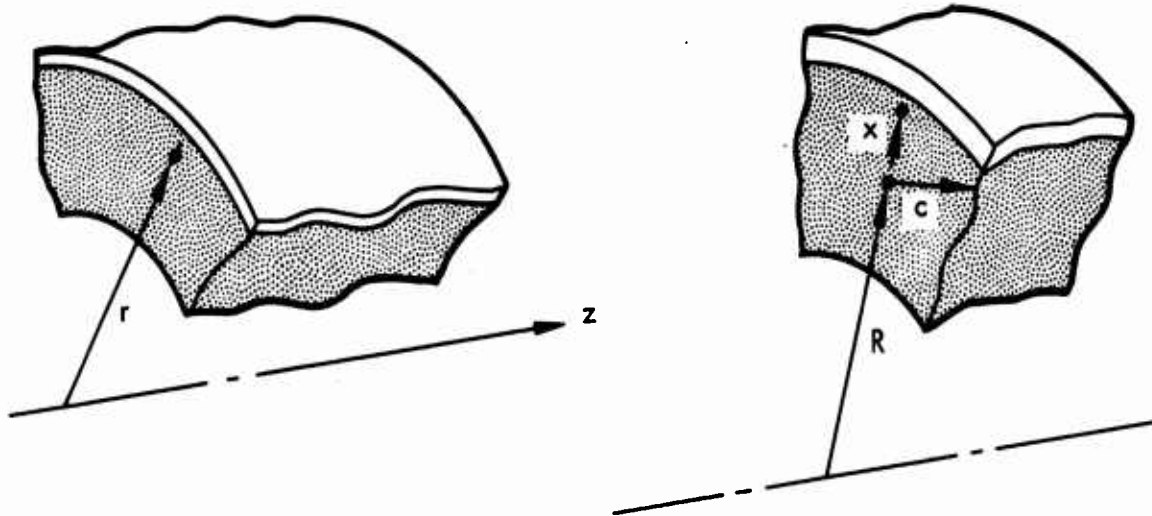The equations of elastic equilibrium of the cylinder, with no body forces may be written as

$$\frac{\partial e}{\partial r} + (1 - 2\nu)\left[\frac{\partial^2 u}{\partial r^2} + \frac{1}{r}\frac{\partial u}{\partial r} - \frac{u}{r^2} + \frac{\partial^2 u}{\partial z^2}\right] = 0$$

$$\frac{\partial e}{\partial r} + (1 - 2\nu)\left[\frac{\partial^2 w}{\partial r^2} + \frac{1}{r}\frac{\partial w}{\partial r} + \frac{\partial^2 w}{\partial z^2}\right] = 0 \quad,$$

where

$$e = \epsilon_r + \epsilon_\theta + \epsilon_z = \frac{\partial u}{\partial r} + \frac{u}{r} + \frac{\partial w}{\partial z} \quad.$$

Let $r = R + x$

and $\qquad \xi = \frac{x}{c} \quad, \quad \eta = \frac{z}{c} \quad;$

also, put

$$\epsilon = \frac{c}{R} \quad.$$

For the coordinate transformation, the first equation could be rewritten as

$$\frac{\partial}{\partial \xi} \left(\frac{\partial u}{\partial \xi} + \frac{\partial w}{\partial \eta} + \frac{u \, \epsilon}{1 + \eta \epsilon}\right) + (1 - 2\nu)\left[\frac{\partial^2 u}{\partial \xi^2} + \frac{\partial u}{\partial \xi} \, \frac{\epsilon}{1 + \xi \epsilon} + \frac{\partial^2 u}{\partial \eta^2} - \frac{u \, \xi}{(1 + \xi \epsilon)^2}\right] = 0$$

Assuming $c \rightarrow \theta$ and, thus, $\epsilon \rightarrow 0$ and neglecting higher order terms gives

$$\frac{\partial}{\partial \xi} \left(\frac{\partial u}{\partial \xi} + \frac{\partial w}{\partial \eta}\right) + (1 - 2\nu)\left[\frac{\partial^2 u}{\partial \xi^2} + \frac{\partial^2 u}{\partial \eta^2}\right] = 0$$

which is identical to the plane-strains solution. Therefore, the displacements and stress in a small region of a cylindrical coordinate system are the same as plane strain problems, provided the same boundary conditions exist.

2.3 DEFECT ANALYSIS

The analysis of stress and strain in linear viscoelastic bodies is considered applicable when an analysis of a solid rocket motor propellant grain is in question. A typical case where a viscoelastic solution can be applied is that of a void defect in a propellant grain. As the internal surface burns, the void can only experience the stresses resulting from the pressure loading. But suppose, by some means, the void was to ignite. The occurrence of ignition prior to the inner burning surface reaching the void would cause added stresses in the immediately surrounding area.

It is assumed, therefore, that the defect is represented by a spherical cavity in an infinite linear viscoelastic media. At some time the surface of the void is subjected to pressure transient. Inertia effects are to be included in the analysis. No thermal effects are to be included either in mechanical and physical properties or in the thermal stress field. This investigation is of interest to support the continuing defect analysis under the Nondestructive Testing (NDT) program. In addition, this presentation may show possible areas of analysis not considered heretofore.

2.3.1 Stress Equilibrium

The equilibrium equation expressed in spherical coordinates for axisymmetrical loading condition has the form (Reference 20):

$$\frac{\partial \sigma_r}{\partial r} + \frac{2}{r} \left(\sigma_r - \sigma_\theta \right) + R = 0 , \tag{78}$$

where R is a body force.

To include the inertia effects, the body force can be expressed as

$$R = -\rho \, \frac{\partial^2 u}{\partial t^2} \quad , \tag{79}$$

where
$$\rho = \text{mass density}$$
$$u = \text{radial displacement} \, .$$

In order that a relationship between the displacements and the stresses be defined, it is required that the special distribution of the space and time variations be separable. A convenient way to remove this dependence is to apply the Laplace transform:

$$\overline{F}(X, \, s) = \int_0^\infty f(X, \, t) \, e^{-st} \, dt \quad , \tag{80}$$

where $f(X, \, t)$ is real and

$$f(X, \, t) = \frac{\text{Re}}{\pi} \int_0^\infty \overline{f}(X, \, s) \, e^{st} \, ds \, . \tag{81}$$

It can be shown that the removal of the time variable allows the application of the already developed theories of elasticity. Thus, the extensive literature of elasticity can be utilized in the viscoelastic analysis. Applying the Laplace transform to Equation 78 gives

$$\frac{\partial \overline{\sigma}_r}{\partial r} + \frac{2}{r} \left(\overline{\sigma}_r - \overline{\sigma}_\theta \right) = \rho \, s^2 \overline{u} \quad , \tag{82}$$

where ($\bar{}$) refers to the transformed state

and s = operator .

From elasticity theories (Reference 5), the displacement, $\bar{u}$, is related to the stresses, $\bar{\sigma}$, as follows:

$$\bar{\sigma}_r = \bar{\lambda} \left(\frac{\partial \bar{u}}{\partial r} + \frac{2 \bar{u}}{r} \right) + 2 \bar{\mu} \frac{\partial \bar{u}}{\partial r}$$

$$\bar{\sigma}_\theta = \bar{\lambda} \left(\frac{\partial \bar{u}}{\partial r} + \frac{2 \bar{u}}{r} \right) + 2 \bar{\mu} \frac{\bar{u}}{r} \quad . \tag{83}$$

Substituting Equations 83 into 82, gives the relation

$$\frac{\partial^2 \bar{u}}{\partial r^2} + \frac{2}{r} \frac{\partial \bar{u}}{\partial r} - \frac{2 \bar{u}}{r^2} = \frac{\rho}{\bar{\lambda} + 2\bar{\mu}} s^2 \bar{u} \quad . \tag{84}$$

Rearranging terms, the well-known Bessel's equation is obtained

$$r^2 \frac{\partial^2 \bar{u}}{\partial r^2} + 2r \frac{\partial \bar{u}}{\partial r} - \left[2 + a^2 s^2 r^2 \right] \bar{u} = 0 \quad , \tag{85}$$

where $a^2 = \dfrac{\rho}{\bar{\lambda} + 2\bar{\mu}}$.

The solution to Equation 85 is known (Reference 21) as

$$r^2 \bar{u} = c_1 (asr - 1) e^{asr} + c_2 (asr + 1) e^{-asr} \quad . \tag{86}$$

Since the media is assumed to be infinite, only the decaying function will be used

$$\bar{u} = \frac{c}{r^2} \ (asr + 1)e^{-asr} \ .$$ (87)

The stresses can be determined by substituting Equation 87 into 83

$$\bar{\sigma}_r = \frac{c}{r^3} \left[4\bar{\mu} \ (1 + asr) \ - \rho s^2 r^2 \right] e^{-asr}$$ (88)

$$\bar{\sigma}_\theta = \frac{c}{r^3} \left[2\bar{\mu} \ (1 + asr) + \bar{\lambda} a^2 s^2 r^2 \right] e^{-asr} \ .$$ (88)

To evaluate the constant c , the actual stress at the surface at time $t = 0$ can be represented as

$$\sigma_r \ (r, \ t) \ = \ \sigma_r^0 \ (r_0, \ 0) \ .$$ (89)

Likewise, its transformed function can be defined as

$$\bar{\sigma}_r \ (r, \ s) \ = \ \bar{\sigma}_r^0 \ (r_0, \ s) \ .$$ (90)

Therefore, the coefficient has an expression

$$c \ = \ - \ \frac{\bar{\sigma}_r^0 \ r_0^3 \ e^{asr_0}}{4 \left[\bar{\mu} \ (1 + asr_0) \ - \rho s^2 r_0^2 \right]} \ .$$ (91)

The actual stresses in the body can be expressed therefore as:

$$\sigma_r = \text{Re} \int_0^\infty \bar{\sigma}_r^{\,0} \left(\frac{r_0}{r}\right)^3 \left[\frac{4\bar{\mu}\,(1 + asr) - \rho s^2 r^2}{4\bar{\mu}\,(1 + asr_0) - \rho s^2 r_0^2}\right] e^{asr_0 + st}\, ds$$

$$\sigma_\theta = \text{Re} \int_0^\infty \bar{\sigma}_{r_0}^{\,0} \left(\frac{r_0}{r}\right)^3 \left[\frac{2\bar{\mu}\,(1 + asr) + \bar{\lambda}(asr)^2}{4\bar{\mu}\,(1 + asr_0) - \rho s^2 r_0^2}\right] e^{asr_0 + st}\, ds \quad . \text{(92)}$$

The evaluation of Equations 92 can be performed by either direct or numerical integration. However, in order to evaluate the stresses the transformed Lame constants must be known.

For most materials, especially a solid rocket motor propellant grain, the viscoelastic properties vary between type or class of material so that it is necessary to determine experimentally the properties for each. In order to apply any experimental data to a viscoelastic stress analysis, the response or time interval of the experiment must be the same as the interval of interest.

In addition, the type of experiment and, thus , the phenomenological model assumed is of interest. It has been stated (Reference 22) with good basis that no solid propellant can be simulated by a single Maxwell element. It would appear that a number of Maxwell elements in parallel can more adequately represent the dynamic behavior of propellant grain. With the additional assumption of linear viscoelastic behavior, an approximate model of a finite number of Maxwell elements can be used over a given frequency spectrum.

Welch (Reference 23) describes an asymptotic procedure to approximate the complex modules. This procedure is similar to the Bode (Reference 24) technique used in electrical network synthesis. Citerley (Reference 25) describes a similar procedure, except a digital procedure is used in determining the stiffness of each element. By arbitrarily selecting the time constants of the various elements for the particular range, adequate representation is developed. Once the complex modulus has been determined for tensile as well as shear, a transform of the Lame constants is possible.

After the transformation is accomplished and the stresses in Equation 92 have been evaluated, it remains to combine these results with a criterion for determining if fracture will occur. Unfortunately, no clear failure criterion exists for the propellant grain material.

2.3.2 Fracture Criteria of Viscoelastic Materials

Fracture criteria applicable to triaxial states of stress are seldom available for any material. Determination of such criterion for a given material is a formidable experimental task even for elastic behavior, let alone viscoelastic. Uniaxial data, however, is usually abundant. The possible generalizations of uniaxial data to multiaxial states are numerous and the selection of a particular criterion is more or less arbitrary. In this light, we see that indiscriminant application of such criterion is unreliable and could label as safe, stress states that actually cause fracture.

As an alternative to trying to establish a precise criterion, upper and lower bounds may be found by using fundamental properties of the fracture surface and available uniaxial data.

The fracture envelope for uniaxial tension for various strain rates at constant temperature appears as follows.
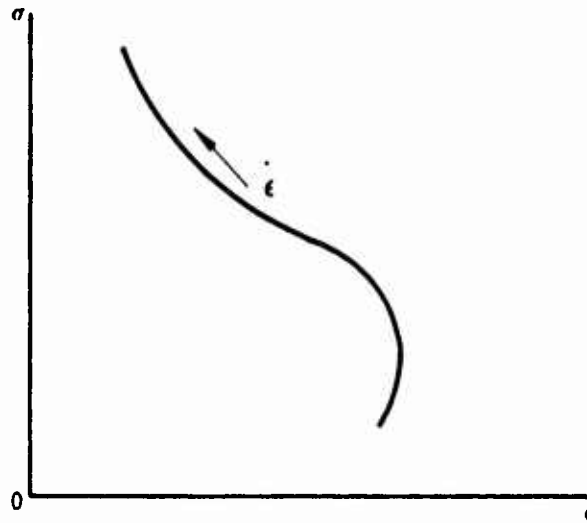
For a given temperature and strain rate, then, let the tensile fracture strength be σ_T . Let the compressive strength be σ_C . If σ_C is not available, we must assume $\sigma_T = \sigma_C$. If the shear strength is given, for which the principal stresses are $(\sigma_S, -\sigma_S)$, an alternate, but similar, procedure to what follows must be used to obtain the fracture spectrum.

Given σ_T and σ_C , consider the fracture criteria to be representable in a three-dimensional space in which the coordinate axes are principal stresses. The intersection of the fracture spectrum with any coordinate plane appears as in Figure 14, where construction lines have been included for clarity.

The assumptions employed in Figure 14 are that the material is isotropic and that the fracture locus varies linearly with hydrostatic pressure. Thus, the spectrum is only partial with respect to hydrostatic stress, but is complete in the octahedral shear plane.
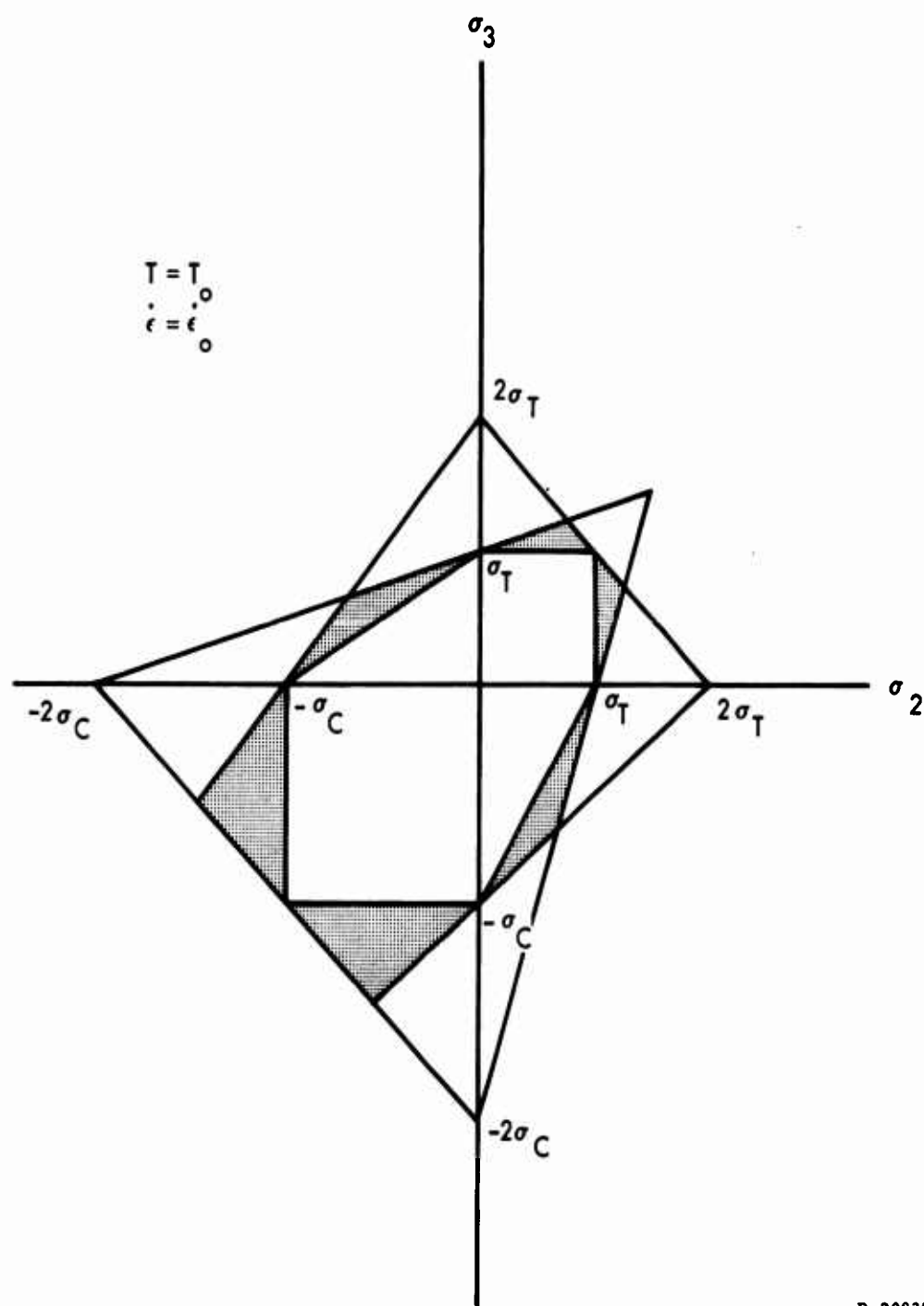
Figure 14.   Fracture Spectrum—Coordinate Plane Intersection

R-20835

2.4 DETERMINATION OF THE PRESSURE DISTRIBUTION IN A PROPELLANT GRAIN CRACK

2.4.1 Analysis

The seriousness of a grain defect may depend on whether or not the defect will propagate or tear when it is exposed to the hot combustion gases and starts to burn. Before determining from a stress analysis, whether the defect will propagate or tear the pressure distribution along the propellant defect must be determined. The purpose of the following analysis is to determine this pressure distribution. The analysis is applicable for a propellant grain crack with variable cross-sectional area.

In the analysis, the following simplifying assumptions are used:

1. Mass is added at a constant flame temperature and at zero velocity

2. The perfect gas equation of state is considered valid

3. The divergence of convergence angle of the propellant grain crack is considered small

4. The flow in the propellant crack is quasi one-dimensional .

Considering a flow volume element as shown in Figure 15, the continuity equation can be expressed as

$$\dot{w}_p = \frac{d\dot{w}}{dx} , \tag{93}$$
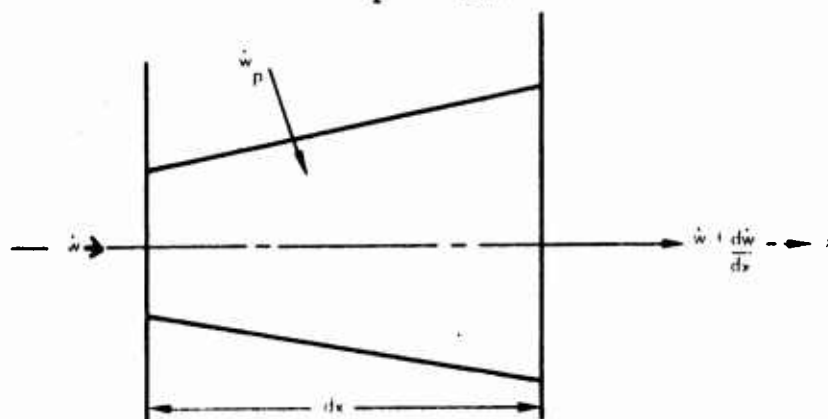
R-20822

Figure 15. Flow Volume Element

the momentum equation as

$$\frac{d}{dx} (\dot{w}V) + \frac{d}{dx} (PA) - P \frac{dA}{dx} - T A_s \quad , \qquad (94)$$

and the conservation of energy equation as

$$\dot{w}_p h_p = \frac{d}{dx} \left(\dot{w} C_p T + \frac{\dot{w} V^2}{2} \right) . \qquad (95)$$

By substituting $\dot{w} = \rho V A$ into Equation 93 and differentiating the product, then

$$\frac{d\rho}{dx} = \frac{\dot{w}_p - \rho A \frac{dV}{dx} - \rho V \frac{dA}{dx}}{VA} \quad . \qquad (96)$$

Likewise, differentiating the products in Equation 94 and solving for $\frac{dP}{dx}$, then

$$\frac{dP}{dx} = \frac{- T A_s - \dot{w} \frac{dV}{dx} - V \dot{w}_p}{A} \quad . \qquad (97)$$

By using the perfect gas equation of state and substituting Equation 97 for $A \frac{dP}{dx}$, then Equation 95 yields, when solved for $\frac{dV}{dx}$

$$\frac{dV}{dx} = \frac{(\gamma - 1) \dot{w}_p h_p + \left(\frac{\gamma - 1}{2}\right) \dot{w}_p V^2 + \gamma T A_s V - \gamma VP \frac{dA}{dx}}{(\gamma PA - \dot{w}V)} . \qquad (98)$$

Equations 96, 97, and 98 were solved on the IBM-1620. Since the two boundary conditions are the velocity at $x = 0$ and the static

pressure at $x = L$, an iterative procedure was used to solve the set of differential equations.

A typical solution of the equations is shown in Figure 16. In this solution, the skin friction force was neglected and the local propellant burning rate was determined from $\dot{r} = b\,P^n$, where P is the local static pressure.
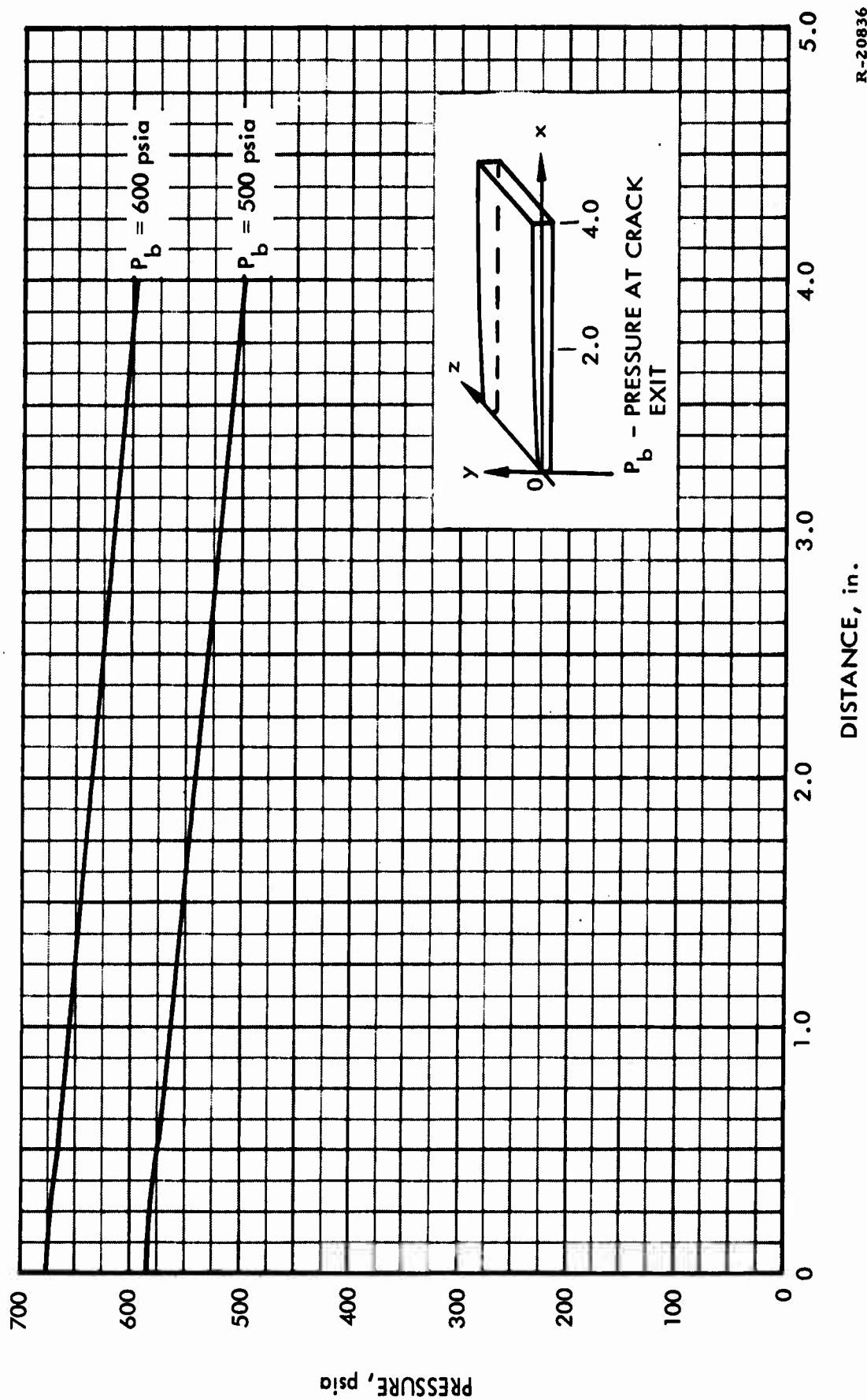
Figure 16. Pressure Distribution in a Grain Crack

## 2.5 TEMPERATURE INCREASE OF THE METAL CASE RESULTING FROM PREMATURE EXPOSURE OF THE CASE INSULATION

The metal case beneath the propellant is protected by a thin slab of insulation. This insulation is usually only exposed to the combustion gases following the completion of the motor firing. However, if a grain defect is present in the propellant (Figure 17), the case insulation may be exposed during the motor firing, causing an increase in the temperature of the metal case. The purpose of this analysis is to present a method to determine this temperature as a function of insulation thickness and time of exposure.

This analysis is applicable only if aerodynamic heating is negligible. For severe aerodynamic heating, the solution of the governing heat transfer equations for the wall temperature must include this effect.

However, since aerodynamic heating is a function of the flight trajectory, a solution to the problem in the form of metal case temperature as a function of insulation thickness and insulation exposure time would be restricted to a particular trajectory. Therefore, by neglecting aerodynamic heating, a general first order estimate of the effect of a particular grain defect on the metal wall temperature can be obtained.

In determining the temperature of the metal case as a function of insulation thickness and insulation exposure time, the following simplifying assumptions are employed:

1. Newtonian heating of the steel case
2. Thermal properties of the insulation and steel case are invariant with temperature
3. One-dimensional heat transfer
4. Steel case perfectly insulated at $x = L$
5. No thermal resistance between the steel case and insulation
6. Uniform initial temperature
7. Uniform thermal film resistance on the surface of the insulation .
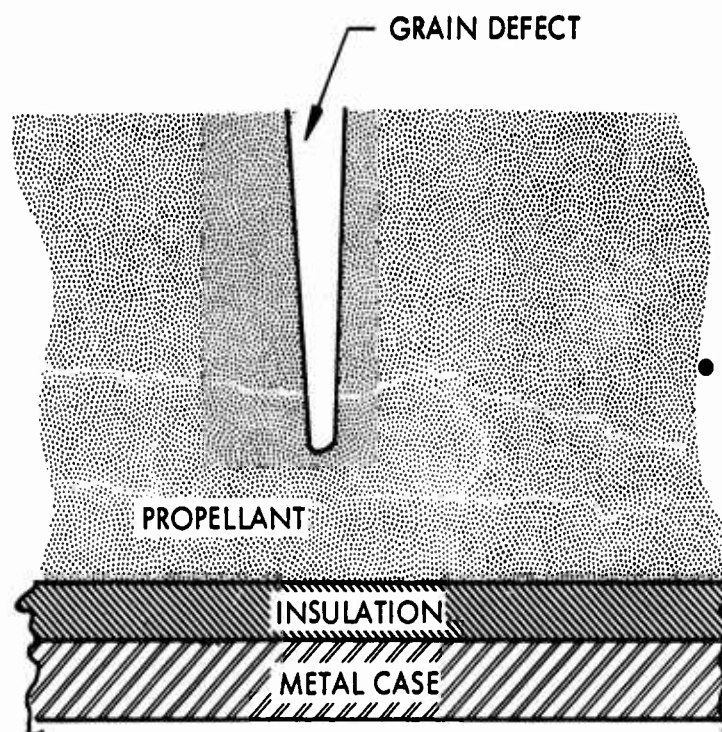
Figure 17. Hypothetical Grain Defect

Using the above assumptions, the system to be analyzed is shown in Figure 18.

The governing partial differential equation for heat conduction is

$$K \frac{\partial^2 T}{\partial x^2} = \rho \ C \ \frac{\partial T}{\partial t} \quad . \qquad (99)$$

The boundary conditions for the differential equation are:
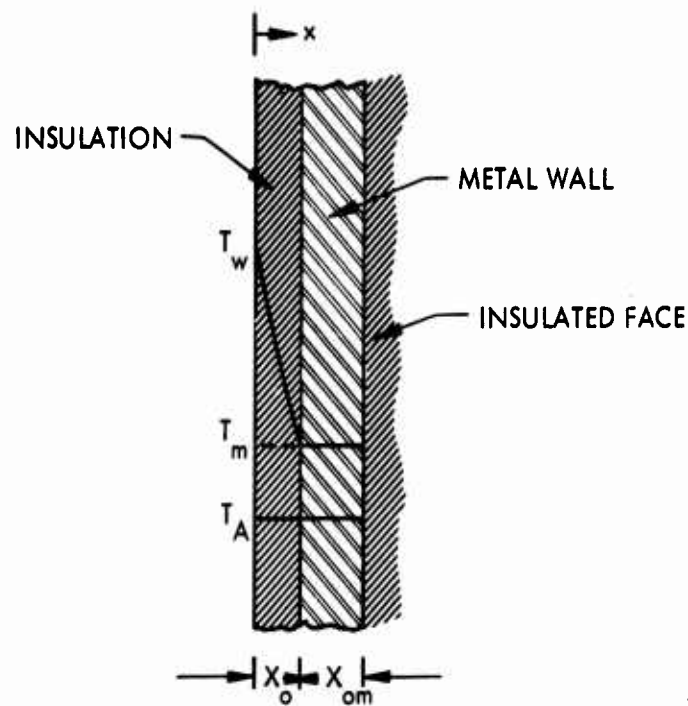
$$T = T_A \ \text{at} \ t = 0 \qquad (100)$$

$$T = T_c \ \text{as} \ t \longrightarrow \infty \qquad (101)$$

$$-K \frac{\partial T}{\partial X} = h \ (T_c - T_w) \ \text{at} \ x = 0 \qquad (102)$$

$$-K \frac{\partial T}{\partial X} = \rho_m \ C_m \ X_{om} \ \frac{\partial T}{\partial t} \ \text{at} \ x = X_o \quad . \qquad (103)$$

where the subscript m refers to the metal case.

R-20838

Figure 18. Heat Transfer Model to be Analyzed

The solution (Reference 26) to Equations 99 through 103 is

$$\frac{T_c - T}{T_c - T_A} = \sum_{i=1}^{\infty} \frac{2be^{-\alpha a_i^2 t}\left(a_i^2 + g^2\right)\left(b \sin a_i X_o + a_i \cos a_i X_o\right)}{a_i\left\{\left[\left(bg - a_i^2\right)^2 + a_i^2 (b+g)^2\right]X_o + \left(bg + a_i^2\right)(b+g)\right\}} \qquad (104)$$

where $\quad b = \dfrac{h}{K}$, $\quad g = \dfrac{\rho C}{\rho_m C_m X_{om}}$, $\quad a = \dfrac{K}{\rho C}$

and $\quad a_i$ = positive roots of $\tan a_i x_0 = \dfrac{\dfrac{b}{g} - a_i^2}{(b+g)a_i}$

Using the following data and solving for T at $x = x_0$, the data shown on Figure 19 was obtained. The solution, obtained on the IBM-1620, is for material thicknesses corresponding to the five-segment, 120-inch motor with the following material properties:

Typical Insulating Material	D6AC Steel

$C = 0.35$ BTU/lb ^{o} F $C_m = 0.113$ BTU/lb ^{o} F

$\rho = 0.0437$ lb/cu in. $\rho_m = 0.283$ lb/cu in.

$K = 2.13 \times 10^{-6}$ BTU/sec ^{o} F in.
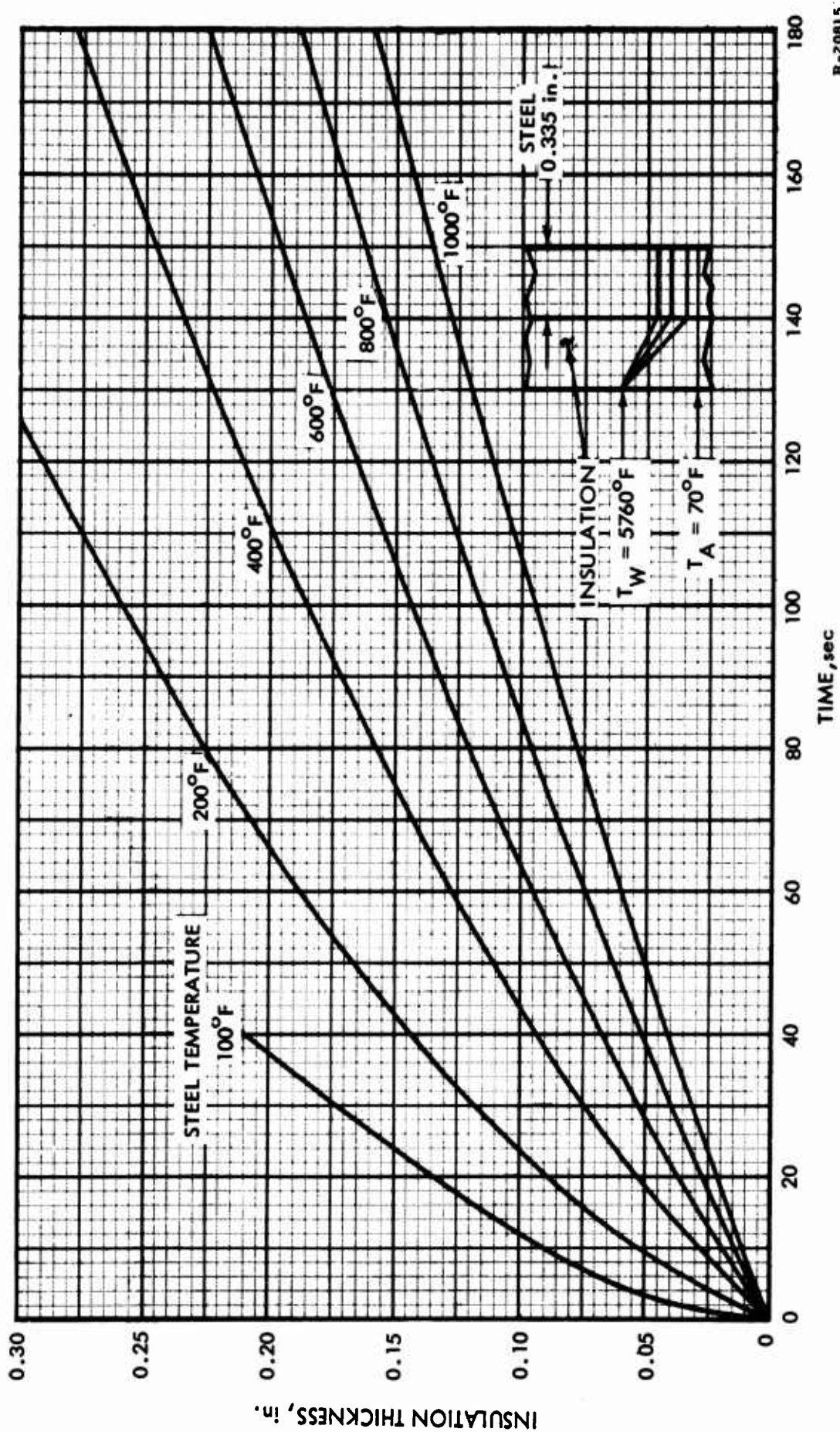
Figure 19. Insulation Thickness Required versus Time for Various Steel Temperatures

2.6 METHOD FOR DETERMINING THE BURNING PROPELLANT SURFACE AREA AS A FUNCTION OF TIME BASED ON AN EXPERIMENTAL COMBUSTION CHAMBER PRESSURE

In analyzing a motor firing in which the propellant grain contained numerous defects, the trace of the combustion chamber pressure can be used to determine the burning propellant surface area as a function of time. By comparing this burning surface area against the burning surface for the grain without defects, the effective burning surface area in the defect can be determined approximately.

The system control volume used in the analysis is shown in Figure 20 and is used along with the following assumptions to obtain the governing equations for the flow model:

A. Assume the perfect gas equation of state is applicable

B. Assume perfect mixing in the combustion chamber

C. Assume the C_p, C_v, and γ of the propellant combustion products in the igniter are the same as for the propellant combustion products in the main motor and that they are constant

D. Assume quasi-steady flow and one dimensional isentropic flow through the nozzle

E. Assume the heat flux to the propellant in the motor is negligible

F. Assume the nozzle throat of the igniter is choked initially

G. Assume viscous effects are negligible

H. Assume the velocity of the gases at the nozzle entrance is negligible in comparison with the velocity from the nozzle exit .

Due to the transient nature of the ignition process, the governing equations which are used to define the flow model depend on whether or not the nozzle throat of the main motor and the igniter are choked and whether or not the
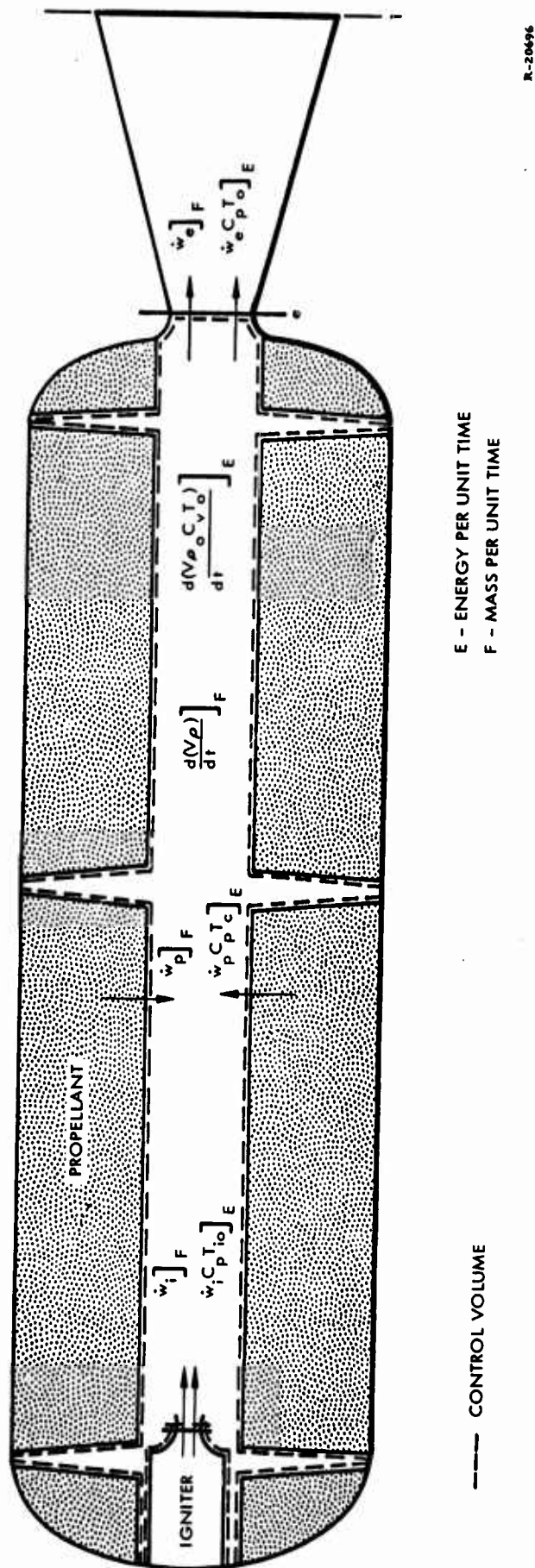
Figure 20. Flow Model

propellant in the main motor is burning. Depending on the flow conditions, the analysis includes the following regimes:

1. The nozzle throat of the igniter is choked but the nozzle throat of the main motor is not choked, and the propellant in the main motor is not burning. The governing equations are

$$\dot{w}_i \, T_{io} = \dot{w}_e \, T_o + \frac{V}{\gamma R} \, \dot{P}_o \tag{105}$$

$$\dot{w}_i = \dot{w}_e + V \dot{\rho}_o \tag{106}$$

$$\dot{w}_e = \sqrt{\frac{g\gamma}{R}} \; \frac{P_o}{T_o} \; \frac{A_1 M_1}{\left(1 + \frac{\gamma - 1}{2} M_1^2\right)^{\frac{\gamma + 1}{2(\gamma - 1)}}} \tag{107}$$

$$\frac{P_o}{\rho_o} = R \, T_o \tag{108}$$

$$\frac{P_o}{P_1} = \left(1 + \frac{\gamma - 1}{2} M_1^2\right)^{\frac{\gamma}{\gamma - 1}} \tag{109}$$

$$\dot{w}_i = A_i \sqrt{\frac{g\gamma}{R} \left(\frac{2}{\gamma + 1}\right)^{\frac{\gamma + 1}{\gamma - 1}}} \; \frac{P_{io}}{\sqrt{T_{io}}} \tag{110}$$

2. The nozzle throat of both the igniter and main motor are choked, and the propellant in the main motor is not burning. The governing equations are

$$\dot{w}_i \, T_{io} = \dot{w}_e \, T_o + \frac{V}{\gamma R} \, \dot{P}_o$$

$$\dot{w}_i = \dot{w}_e + V \dot{\rho}_o$$

$$\dot{w}_e = A_e \sqrt{\frac{g\gamma}{R} \left(\frac{2}{\gamma + 1}\right)^{\frac{\gamma + 1}{\gamma - 1}}} \; \frac{P_o}{\sqrt{T_o}} \qquad (111)$$

$$\frac{P_o}{\rho_o} = R \, T_o$$

$$\dot{w}_i = A_i \sqrt{\frac{g\gamma}{R} \left(\frac{2}{\gamma + 1}\right)^{\frac{\gamma + 1}{\gamma - 1}}} \; \frac{P_{io}}{\sqrt{T_{io}}}$$

3. The nozzle throat of both the igniter and main motor are choked, and the propellant in the main motor is burning. The governing equations are

$$\dot{w}_i T_{io} + \dot{w}_p T_c = \dot{w}_e T_o + \frac{V}{\gamma R} \dot{P}_o \qquad (112)$$

$$\dot{w}_i + \dot{w}_p = \dot{w}_e + V \dot{\rho}_o \qquad (113)$$

$$\dot{w}_e = A_e \sqrt{\frac{g\gamma}{R} \left(\frac{2}{\gamma + 1}\right)^{\frac{\gamma + 1}{\gamma - 1}}} \frac{P_o}{\sqrt{T_o}}$$

$$\dot{w}_p = b P_o^n \rho_b A_s \qquad (114)$$

$$\frac{P_o}{\rho_o} = R T_o$$

$$\dot{w}_i = A_i \sqrt{\frac{g\gamma}{R} \left(\frac{2}{\gamma + 1}\right)^{\frac{\gamma + 1}{\gamma - 1}}} \frac{P_{io}}{\sqrt{T_{io}}} \qquad (115)$$

4. The nozzle throat of the igniter is not choked but the nozzle throat of the main motor is choked, and the propellant in the main motor is burning. The governing equations are

$$\dot{w}_i \, T_{io} + \dot{w}_p \, T_c = \dot{w}_e \, T_o + \frac{V}{\gamma R} \, \dot{P}_o$$

$$\dot{w}_i + \dot{w}_p = \dot{w}_e + V \dot{\rho}_o$$

$$\dot{w}_e = A_e \sqrt{\frac{g\gamma}{R} \left(\frac{2}{\gamma + 1}\right)^{\frac{\gamma + 1}{\gamma - 1}}} \; \frac{P_o}{\sqrt{T_o}}$$

$$\dot{w}_p = b \, P_o^{\,n} \, \rho_b \, A_s$$

$$\frac{P_o}{\rho_o} = R \, T_o$$

$$\frac{P_{io}}{P_o} = \left(1 + \frac{\gamma - 1}{2} \, M_i^2\right)^{\frac{\gamma}{\gamma - 1}} \tag{116}$$

$$\dot{w}_i = A_i \sqrt{\frac{g\gamma}{R}} \; \frac{P_{io}}{\sqrt{T_{io}}} \; \frac{M_i}{\left(1 + \frac{\gamma - 1}{2} \, M_i^2\right)^{\frac{\gamma + 1}{2(\gamma - 1)}}} \tag{117}$$

The equations in each regime were solved numerically on the IBM-1620 computer.

A typical solution to the equations is shown in Figure 21 for a large rocket motor. This motor did not contain any grain defects.
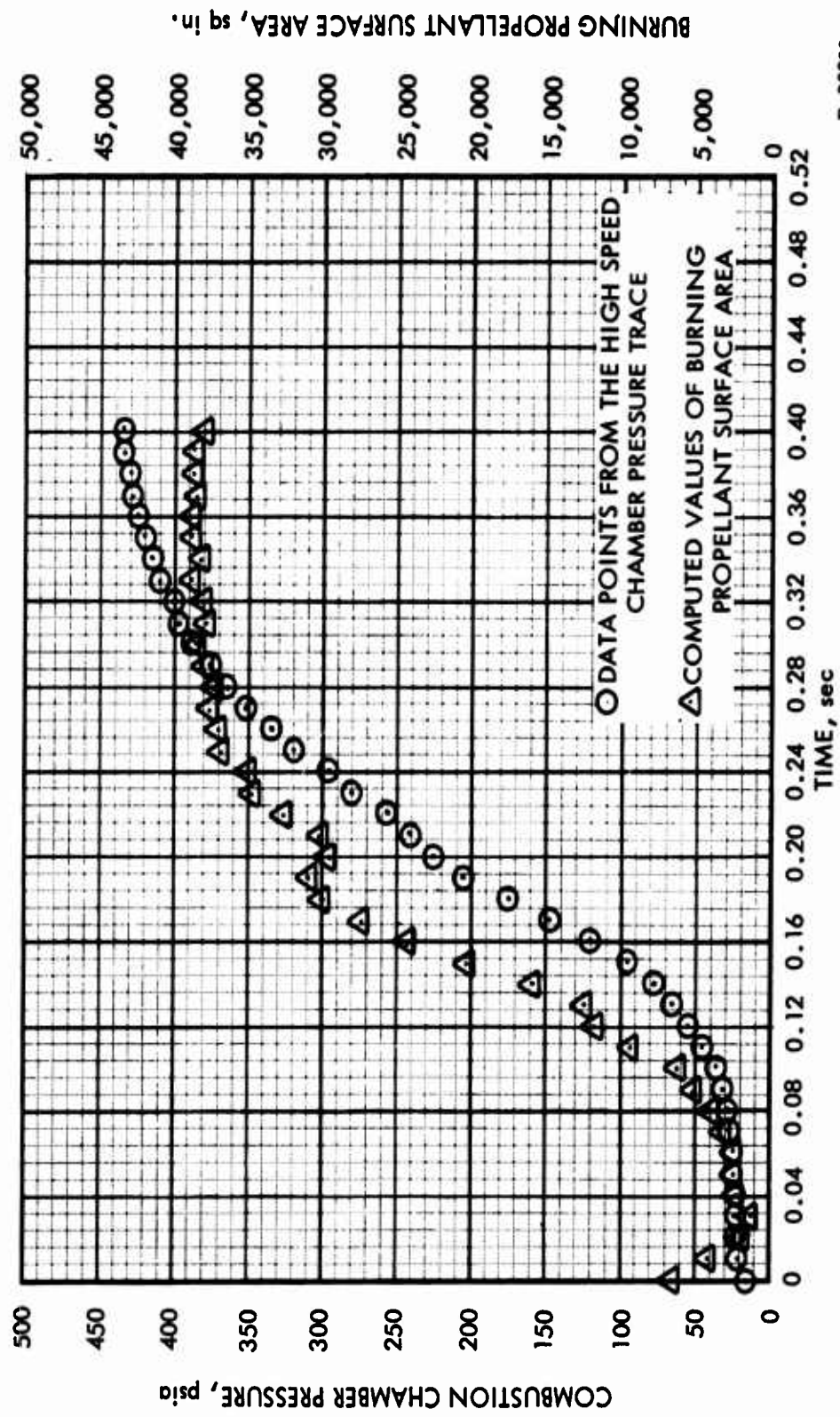
Figure 21. Calculated Burning Propellant Surface Area of a Large Solid Rocket Motor

3.0 REFERENCES

1. Geckler, R. D., "Thermal Stresses in Solid Propellant Grain," Jet Propulsion, February 1956, p. 93.

2. Ungar, E. E., and B. W. Shaffer, "Thermally Induced Bond Stresses in Case-Bonded Propellant Grains," ARS Journal, April 1960, p. 366.

3. Au, N. N., "A Method of Strength Analysis of Solid Propellant Grains," ARS Paper 1062-60.

4. Knauss, Wolfgang, "Displacements in a Tubular Rocket Grain Under Axial Acceleration," GALCIT SM 61-10, Guggenheim Aero. Lab., CIT, Pasadena, California, April 1961.

5. Pickett, Gerald, "Application of the Fourier Method to the Solution of Certain Boundary Problems in the Theory of Elasticity," Journal of Applied Mechanics, Vol. 11, September 1944, p. A-176.

6. Conte, S. D., K. L. Miller, and C. B. Sensenig, "The Numerical Solution of Axisymmetric Problems in Elasticity," Proc. of 5th Symp. on Ballis. Missiles and Sp. Tech., Vol IV, Academic Press, 1960.

7. Messner, A. M., "Propellant Grain Stress Analysis," Bulletin of 17th Meeting JANAF-ARPA-NASA, Vol. II, May 1961, p. 149.

8. Timoshenko, S. and J. N. Goodier, Theory of Elasticity, 2nd Ed., McGraw-Hill, 1951, p. 408.

9. Williams, M. L., P. J. Blatz, R. A. Schapery, "Fundamentals Studies Relating to Systems Analysis of Solid Propellants," Report No. GALCIT SM 61-5, Guggenheim Aero. Lab. CIT, Pasadena, California, February 1961.

10. Aleck, B. J., "Thermal Stresses in a Rectangular Plate Clamped Along an Edge," Trans. ASME Vol. 71, 1949, p. A-118.

11. Courant, R., and D. Hilbert, Methods of Mathematical Physics, Vol. I, Interscience Publishers, Inc., New York, 1955.

12. Lanczos, C., The Variational Principles of Mechanics, Vol. 4, Mathematical Expositions, Univ. of Toronto Press, Toronto, Ontario, 1960.

13. Frazer, R. A., W. Duncan, and A. R. Collar, Elementary Matrices, Cambridge, 1952, p. 157.

14. Barton, M. V., Journal of Applied Mechanics, Vol. 8, 1941, p. A-97.

15. Horvay, G. and J. A. Mirbal, "The End Problem of Cylinders," Journal of Applied Mechanics, Vol. 25, December 1958, p. 561.

16. Kent, C. H., "Thermal Stresses in Thin Wall Cylinders," Journal of Applied Mechanics, APM-53-13.

17. Durelli, A. J. and C. H. Tsao, "Determination of Thermal Stresses in Three-ply Laminates," Journal of Applied Mechanics, Vol. 22, 1955, p. 190.

18. Zandman, F., S. S. Redner, and D. Post, "Photoelastic Coating Analysis in Thermal Fields," to be published ESA; First International Symposium on Photoelasticity, 1961.

19. Williams, M. L., "Stress Singularities Resulting from Various Boundary Conditions in Angular Corners of Plates in Extension," Journal of Applied Mathematics, Vol. 19, 1951, p. 526.

20. Love, A. E. H., A Treatise on the Mathematical Theory of Elasticity, Dover, 1944, p. 249.

21. Pickett, S., "Fourier Method to the Solution of Certain Boundary Problems in the Theory of Elasticity," Journal of Applied Mechanics, 1944, p. A-176.

21. Kamke, E., Differential Gleichungen-Losungs-Methoden und Losungen, 3rd ed., Chelsea, 1959, 1. 444.

22. Stanford, E. G., and L. H. Fearon, Progress in Non-Destructive Testing, Vol. 2, MacMillan, 1960, p. 39.

23. Welch, J., Jr., "Empirical Determination of Some Mathematical Models in Viscoelasticity," N. Carolina St. DA-01-009-ORD-991, ERD 148/1, August 1961.

24. Truxal, J., Control Synthesis, McGraw-Hill, 1955.

25. Citerley, R., "An Investigation to Simulate the Linear Viscoelastic Behavior of an Elastomer," MS Thesis, USNPS, 1961.

26. Grover and Holter, "Solution of the Transient Heat Conduction Equation for an Insulated, Infinite Metal Slab," ARS Journal, December 1957, p. 1249.

UNCLASSIFIED